Plant Physiol. (1996) 111: 73–92

The Refined Three-Dimensional Structure of Pectate Lyase E from *Erwinia chrysanthemi* at 2.2 Å Resolution[1]

Susan E. Lietzke[2], Robert D. Scavetta, Marilyn D. Yoder[3], and Frances Jurnak*

Department of Biochemistry, University of California, Riverside, California 92521

The crystal structure of pectate lyase E (PelE; EC 4.2.2.2) from the enterobacteria *Erwinia chrysanthemi* has been refined by molecular dynamics techniques to a resolution of 2.2 Å and an R factor (an agreement factor between observed structure factor amplitudes) of 16.1%. The final model consists of all 355 amino acids and 157 water molecules. The root-mean-square deviation from ideality is 0.009 Å for bond lengths and 1.721° for bond angles. The structure of PelE bound to a lanthanum ion, which inhibits the enzymatic activity, has also been refined and compared to the metal-free protein. In addition, the structures of pectate lyase C (PelC) in the presence and absence of a lutetium ion have been refined further using an improved algorithm for identifying waters and other solvent molecules. The two putative active site regions of PelE have been compared to those in the refined structure of PelC. The analysis of the atomic details of PelE and PelC in the presence and absence of lanthanide ions provides insight into the enzymatic mechanism of pectate lyases.

Extracellular pectate lyases are secreted by plant pathogenic microbes and those from the erwinias are believed to be the major virulence factor causing soft rot diseases in plants (Collmer and Keen, 1986; Kotoujansky, 1987). The enzymes attack the plant cell wall and cleave PGA, the major component of the plant cell wall. The best studied are those from *Erwinia chrysanthemi*, which expresses up to five independently regulated genes coding for five isozymes of pectate lyases. All extracellular pectate lyases can be grouped into two subfamilies according to their pIs (Collmer and Keen, 1986; Barras et al., 1987). Those with an acidic or alkaline pI belong to the *pelADE* subfamily, and those with a neutral pI belong to the *pelBC* subfamily. Pectate lyases invoke a β-elimination mechanism to cleave PGA at a pH optimum in the range of 8 to 10 (Kotoujansky, 1987). However, the details of the mechanism with respect to endo- or exolytic cleavage, as well as the length of the end product, differ for each pectate lyase. *E. chrysanthemi* PelE, the subject of the present study and the most virulent of all pectate lyases, is reported to cleave PGA both endo- and exolytically to a dimeric end product (Preston et al., 1992).

An understanding of the pectate lyases has been advanced considerably by the recent structural determinations of three pectate lyases, *E. chrysanthemi* PelC (Yoder et al., 1993a), *E. chrysanthemi* PelE (Lietzke et al., 1994), and *B.s.* Pel (Pickersgill et al., 1994). The polypeptide backbone of all three enzymes form a single domain comprising parallel β strands that are wound into a large, right-handed coil, termed a parallel β helix. In addition to the novel fold, the enzymes share other unique structural features, including a highly organized core consisting of linear arrays of all side chains that are oriented toward the interior (Yoder et al., 1993b). Although the core topology is similar, the three pectate lyases differ substantially in the number, size, and conformation of the loops that protrude from the central core. The loops fold over the exterior surface of the parallel β helix and confer a unique shape and charge on each pectate lyase. Because there is a paucity of biochemical data regarding the amino acids involved in catalysis, the pectinolytic active site could not be identified unambiguously from the three-dimensional structure. Additional clues have been sought and found in an analysis of the amino acid sequences of related proteins.

E. chrysanthemi pectate lyases share sequence similarities with other extracellular pectate lyases. The sequence similarities extend to three well-known patterns of identities: the AxDIKGxxxxVTxS region, the vWiDH motif, and the vxRxPxxRxxxxHxxxN region (Hinton et al., 1989; Hugouvieux-Cotte-Pattat and Robert-Baudouy, 1992; Barras et al., 1994). The overall sequence identity is greater than 50% within each pectate lyase subfamily but much lower between subfamilies. PelE and *E. chrysanthemi* PelC

[1] This work was supported by the U.S. Department of Agriculture (grant no. 94–37303–0730); Academic Computing Graphics and Visual Imaging Lab, University of California, Riverside; and the San Diego Supercomputer Center.

[2] Present address: Department of Chemistry and Biochemistry, University of Colorado at Boulder, Campus Box 215, Boulder, CO 80309–0215.

[3] Present address: School of Biological Sciences, University of Missouri-Kansas City, 010 Biological Sciences Building, 5100 Rockhill Road, Kansas City, MO 64110–2499.

* Corresponding author; e-mail jurnak@citrus.ucr.edu; fax 1–909–787–3590.

Abbreviations: B factor, isotropic temperature factor; *B.s.* Pel, *Bacillus subtilis* pectate lyase; χ, rotation angle about side-chain bonds; crystallographic R factor, agreement factor between observed structure factor amplitudes, F_o, and calculated structure factor amplitudes, F_c, based on the atomic model; F, structure factor; F_c, calculated structure factor; F_o, observed structure factor; PelC, pectate lyase C from *E. chrysanthemi*; PelE, pectate lyase E from *E. chrysanthemi*; PGA, polygalacturonic acid; ϕ, rotation angle about the nitrogen-carbon α bond; ψ, rotation angle about the carbon α-bond; r.m.s., root-mean-square; σ_A, a combined measure of the completeness and accuracy of the partial structure as calculated by the method of Read (1986).

are reported to share 27% sequence identity using evolutionary-based sequence alignment procedures (Hinton et al., 1989), but they share only 20% identity by alignment of the three-dimensional structures (Heffron et al., 1995). Despite the rather low sequence identity between PelE and PelC, the three-dimensional structures are very similar. Moreover, a distantly related pectate lyase from *Bacillus subtilis* has also been shown to have a similar fold (Pickersgill et al., 1994), suggesting that all proteins with certain sequence signatures are likely to have a similar structure. This group includes all extracellular pectate lyases, with the exception of *Fusarium solani* pectate lyase (Gonzales-Candelas and Kolattukudy, 1992), as well as fungal pectin lyases (Gysler et al., 1990; Kuster-Van Someren et al., 1992), and pollen and style plant proteins (Wing et al., 1989; Budelier et al., 1990; Rafner et al., 1991; Rogers et al., 1992). The structural similarities may or may not extend to functional similarities, depending on the sequence similarities in the active site regions. Unfortunately, none of the amino acids involved in PGA cleavage have been identified. A recent analysis of pectate lyase sequences indicates that the invariant "potentially catalytic" residues cluster in two well-separated regions in the pectate lyase structures, suggesting the possibility of two different active sites (Heffron et al., 1995; Henrissat et al., 1995). One is undoubtedly the pectinolytic active site, but the enzymatic function for the second site is unknown.

All extracellular pectate lyases require Ca^{2+} for in vitro activity but its role in catalysis has not been determined (Collmer and Keen, 1986; Kotoujansky, 1987). The three-dimensional structural analysis of *B. subtilis* pectate lyase has revealed a Ca^{2+}-binding site comprising invariant and conserved amino acids on the protein (Pickersgill et al., 1994). It is the same site predicted to be a Ca^{2+}-binding site by lanthanide-binding studies in the PelE and PelC structures (Yoder et al., 1993a; Lietzke et al., 1994). In all three proteins, the Ca^{2+}-binding site lies in a groove suggestive of a saccharide-binding site and is the probable location of the pectinolytic active site. Studies with PelC have demonstrated that a lutetium ion not only inhibits pectinolytic activity but induces a structural rearrangement of ligands around the Ca^{2+} site (Yoder and Jurnak, 1995). A similar analysis but with different results is reported herein for the refined model of PelE. In addition, the atomic details of PelE and PelC in the region of the Ca^{2+} site and the second potential active site around the vWiDH sequence are compared in detail. The analysis suggests functional roles for some of the invariant and conserved residues in the pectate lyases.

MATERIALS AND METHODS

Protein Purification and Activity Assays

PelE was purified from high-expression plasmid constructs of the *pel748*, a *pelE* gene from *Erwinia chrysanthemi* strain EC16 expressed in *Escherichia coli* HB-101 cells (Tamaki et al., 1988). The recombinant form has the same calculated molecular weight, 38,069, and enzymatic properties as the enzyme from natural sources. Enzymatic activity was determined by monitoring the change in A_{232} of sodium polygalacturonate (Keen et al., 1984). The assay solution contained 0.865 mL of 58 mM bis-Tris propane, pH 9.0, 0.005 mL of 0.1 M $CaCl_2$, and 0.125 mL of 1% (w/v) sodium PGA (Sigma). The assay was initiated by the addition of 0.005 mL of appropriately diluted PelE and the A_{232} was recorded every 10 s. One unit of pectate lyase activity is defined as the production of 1 mmol of unsaturated product per min. The formation of 1 mmol of unsaturated uronide per min was taken to correspond to 1.73 A_{232} units per min (Zucker and Hankin, 1970). For the lanthanide inhibition assays, the volume of the initial buffer was reduced to 0.860 mL. After the reaction had proceeded to 0.3 A_{232}, 0.005 mL of $CaCl_2$, $LaCl_3$, or $LuCl_3$ was added to a predetermined concentration to bring the final volume to 1.0 mL.

Crystals and Data Collection

Microcrystals of PelE were grown at 4°C from PEG 3350 in space group $P2_12_12_1$ with a = 38.79 Å, b = 91.14 Å, and c = 102.99 Å (Kim et al., 1989) and enlarged to 0.15 × 0.40 × 0.80 mm by microseeding techniques for data collection (Fitzgerald and Madsen, 1986). The PelE-La^{3+} complex was prepared by adding 0.6 mM $LaCl_3$ to the initial crystallization conditions, and crystals were grown as described for the native PelE crystals. The cell constants of the PelE-La^{3+} crystals were identical with the native PelE crystals. X-ray data were collected on a dual chamber San Diego Multiwire Systems (San Diego, CA) area detector system to a resolution of 2.2 Å and processed as described previously (Lietzke et al., 1994). The PelE-La^{3+} diffraction data were scaled to the native data with a conventional scaling R factor of 12.4%. The native PelE structure was solved by multiple isomorphous replacement techniques using $LaCl_3$, $UO_2(NO_3)_2$, K_2PtCl_4, and KI/Iodo-gen (Sigma), the first two of which shared a common site.

The Refinement Method

The initial PelE protein model was built and partially refined as described earlier (Lietzke et al., 1994). Molecular dynamics techniques were used for refinement using the method of slow-cooling simulated annealing as implemented by X-PLOR (Brünger, 1992). The reflection data were randomly divided into two sets: a working set composed of approximately 90% of the data sampled at random and a test set composed of the remaining 10% of the data used for cross-validation of the refinement cycles (Brünger, 1993). The protein parameters and topology files used in X-PLOR were those based on a survey of the Cambridge Structural Database by Engh and Huber (1991). The weight of the crystallographic term in the molecular dynamics refinement was set to 50% of the value calculated from the empirical "check" procedure of X-PLOR (Brünger, 1993) using the first protein model. This value for the weight was determined subjectively by running several refinements with different fractions of the calculated weight and assessing final model statistics, protein geometry, and model fit to electron density. The weight was kept

constant throughout all except the final set of refinement cycles. The N and C termini and all charged amino acids were given a charge of 0 in each cycle of refinement to prevent them from forming artificial salt bridges with atoms on the surface of the protein.

A cycle of crystallographic refinement consisted of five steps: (a) 120 steps of conjugated gradient minimization using the method of Powell (1977); (b) simulated annealing with a slow-cooling method, starting at 3000 K and cooling to 300 K in 25 K increments; (c) 40 or more steps of conjugated gradient minimization; (d) overall B-factor refinement; and (e) 20 steps of restrained individual isotropic B-factor refinement. Data between 2.2 and 5.0 Å were used in the first two refinement cycles and data between 2.2 and 8.0 Å were used for the third and fourth cycles. Data between 2.2 and 10.0 Å were used in all subsequent refinement cycles. After each refinement cycle the model was checked and manually rebuilt using FRODO (Jones, 1985) or O (Jones et al., 1991), followed by molecular dynamics refinement (Brünger, 1988, 1991). To release all stereochemical restraints, the ninth refinement cycle actually included five complete refinement cycles, each with a gradual increase in the weight of the crystallographic term to the full value initially suggested in the X-PLOR empirical check. Unlike the previous refinement cycles, the model was not adjusted as the weight of the crystallographic term was increased. For the final model (10th refinement cycle) and statistical calculations, all reflections with F greater than 2 SD, including those in the test data set, were used.

After the PelE model was refined to a crystallographic R factor of 20.6% in the fourth refinement cycle, solvent molecules were added in an additional four refinement cycles. Data between 2.2 and 10.0 Å were used in solvent refinement cycles. Each cycle consisted of five steps: (a) automatic assignment of solvent molecules to the top peaks in the F_o-F_c electron density maps using the program MAPMAN (G.J. Kleywegt and T.A. Jones, unpublished data); (b) automatic removal of symmetry-related solvent molecules or those outside the hydrogen-bonding range using the program WATER (Stephen Sprang, personnel communication, 1994); (c) visual verification of remaining solvent molecules for placement in F_o-F_c electron density and meeting reasonable distance and geometry criteria; these waters were given an occupancy of 1; (d) Powell minimization of model with newly identified solvent molecules; and (e) verification of solvent molecules in $2F_o-F_c$ electron density by visual inspection. Solvent molecules were subsequently removed from the model if the B factor exceeded 60 Å^2 or became negative or did not meet reasonable hydrogen-bonding distance and geometry criteria. After each cycle a new F_o-F_c electron density map was calculated and the process of identifying solvent molecules was repeated.

The final PelE coordinates were assumed to be similar to the PelE-La^{3+} complex and were refined, along with the La^{3+} ion, by molecular dynamics techniques described above. The conformations of the amino acids as well as the positions of the solvent molecules around the La^{3+} site were deduced from an F_o-F_c map, in which all atoms within an 8 Å shell around the La^{3+} were omitted from the model calculations. The solvent molecules were assigned as described above and verified by visual inspection of F_o-F_c and $2F_o-F_c$ electron density maps.

The solvent refinement of the PelC and PelC-Lu^{3+} models previously reported (Yoder and Jurnak, 1995) was repeated using the solvent placement procedures described above. The nonsolvent atomic coordinates of the refined PelC and PelC-Lu^{3+} models were used as the initial models and solvent molecules were added in four refinement cycles.

Assignment of Secondary Structural Elements

Secondary structural assignments were made with the algorithm of Kabsch and Sanders (1983) in PROCHECK (Laskowski et al., 1992). Hydrogen bonds were defined by the program HBPLUS (McDonald et al., 1993) using the criteria of Baker and Hubbard (1984), with a donor-acceptor distance of less than 3.9 Å and associated angles greater than 90°. Subsequently, the secondary structural assignments were modified by visual inspection of the main-chain hydrogen bonds. Only those amino acids that had repetitive ϕ and ψ angles characteristic of β conformation and exhibited maximal interstrand hydrogen bonding between main-chain atoms were assigned as β structure in the strands that make up the parallel β-helix core.

Loops were defined as all residues between secondary structural elements in the parallel β-helix core and were characterized according to the nomenclature of Ring et al. (1992). Linear loops are described as strap loops. Nonlinear loops are divided into two categories: planar loops termed ω loops and nonplanar loops termed ζ loops. The definition of an ω loop differs from that of Lesczynki and Rose (1986) in that the ends of the ω loop are not required to be in close proximity.

β turns are loops of four residues or less and are classified according to the nomenclature proposed by Wilmot and Thornton (1990). The criteria for a β turn is (a) $C_{\alpha-i}$ to $C_{\alpha+2}$ distance less than 7 Å and (b) the central amino acids are not part of a helix. The name of the β turn is then derived from the ϕ and ψ backbone dihedral angles. An internal hydrogen bond is not required for a β turn.

Omit Map Calculations

A refined omit map (Bhat and Cohen, 1984; Hodel et al., 1992) was calculated from a model in which all atoms in an 8 Å shell around a specified region had been omitted from the refinement and phase calculation. Atoms within a 3 Å shell around the omitted region were restrained to prevent artificial movement into the unoccupied density. Refinement of the omit model was carried out with a two-step procedure: (a) a round of simulated annealing using a slow-cooling protocol in which the initial temperature was set to 1000 K and (b) conjugate gradient minimization. The region was verified by comparing the model of the $2F_o-F_c$ electron density map calculated from the omit map refinement.

r.m.s. Deviation Calculations

Different regions of the structures of PelE were superimposed and compared to PelC. Although the optimal superposition of the overall structure of both proteins results when the polypeptide backbone of the core elements in the parallel β domain are used, such a superposition does not result in an optimal alignment of individual regions, which include loops. Therefore, to optimize the fit of a specific region, amino acids selected by visual inspection were used. For the vWiDH region, the αCs of the PelE residues 107 to 110, 145 to 148, and 186 to 189 were aligned with the respective αCs of the PelC residues 114 to 117, 142 to 145, and 179 to 182. The r.m.s. fit for the 12 overlapping atoms is 0.31 Å. For the Ca^{2+}-binding site, the αCs of PelE residues 133 to 141, 172 to 182, 196 to 204, 228 to 236, and 258 to 266 were aligned with the respective αCs of the PelC residues 130 to 138, 165 to 175, 189 to 197, 216 to 224, and 239 to 247. The r.m.s. fit for the 47 overlapping atoms is 0.83 Å. A transform was calculated with the least-squares explicit command in O (Jones et al., 1991) by rotating PelC onto PelE and then the transformation matrix was applied to the entire set of PelC coordinates.

Coordinate Deposition

The complete coordinate files of PelE and PelC are being processed by the Brookhaven Protein Data Bank (Bernstein et al., 1977).

RESULTS

Refinement Stages and Progress

Refinement results for PelE for 10 cycles of manual model building followed by molecular dynamics refinement are summarized in Table I. The first four models did not include solvent molecules, and the fourth model is essentially the model described by Lietzke et al. (1994). The fifth, sixth, seventh, and eighth models included 89, 124, 146, and 157 water molecules, respectively. In addition to appropriate distance and geometry criteria, all water molecules appeared in the prerefined F_o-F_c maps contoured at 2.0 SD and the postrefined $2F_o-F_c$ maps contoured at 1.0 SD. The ninth refinement cycle represents a set of refinement cycles in which all stereochemical restraints were gradually released. The 10th refinement cycle used all data with F greater than 2 SD, including the test set.

For the PelE-La^{3+} model, the final PelE coordinates were refined using the PelE-La^{3+} diffraction data set to a crystallographic R factor of 21.9%. After the conformations of all amino acids were adjusted by a series of omit maps, solvent molecules were refined in the same manner as described above for the PelE model. In a similar manner, solvent molecules were added to the PelC and PelC-Lu^{3+} models. In the PelC-Lu^{3+} model, the placement of waters and subsequent refinement revealed three distinct spherical regions of electron density, much too large to accommodate a lone water molecule. The PelC electron density showed only two such regions corresponding to two of the three regions of electron density for the PelC-Lu^{3+} complex. The size and environment of each region of the electron density was compatible with a sulfate ion. Assignment of sulfate ions to the density, followed by a Powell minimization, decreased the crystallographic R factor by 0.6% per sulfate ion. The three regions were sufficiently separated such that the large negative charge of the sulfate ions did not cause errors in the X-PLOR refinement.

Quality of the Final Model

The PelE model described consists of all 355 amino acids and 157 water molecules. In addition to the 355 amino acids, the PelE-La^{3+} complex model includes a La^{3+} ion and 163 water molecules. With the exception of the tips of two extended loops, there is strong connectivity and very clear carbonyl oxygen bulges in the final $2F_o-F_c$ electron density maps contoured at 1.0 SD. Two regions, Glu^{124} to Asp^{127} and Lys^{164} to Glu^{167}, were problematic throughout the analysis of the PelE model. The main chain of the Lys^{164} to Glu^{167} loop finally became reasonably clear in the final σ_A-weighted $2F_o-F_c$ electron density map. There was minimal density for Ser^{125} and Gly^{126}, making it difficult to

Table I. *Summary of the refinement of PelE*

Resolution	Model	R Factor		r.m.s. Deviations			No. of Water Molecules	Residues in Model
		Working	Free	Bond	Angle	Impropers		
Å				Å	°	°		
2.2–5.0	1	0.242	0.314	0.007	1.200	1.920	0	1–123, 128–355
2.2–5.0	2	0.210	0.279	0.007	1.500	1.310	0	1–355
2.2–8.0	3	0.211	0.276	0.007	1.580	1.130	0	1–355
2.2–8.0	4	0.206	0.269	0.006	1.560	1.080	0	1–355
2.2–10.0	5	0.180	0.239	0.006	1.740	1.130	89	1–355
2.2–10.0	6	0.172	0.223	0.006	1.690	1.090	124	1–355
2.2–10.0	7	0.169	0.221	0.006	1.670	1.070	146	1–355
2.2–10.0	8	0.164	0.220	0.007	1.616	1.059	157	1–355
2.2–10.0	9	0.157	0.220	0.009	1.707	1.191	157[a]	1–355
2.2–10.0	10	0.161		0.009	1.721	1.180	157[b]	1–355

[a] One hundred percent of the ideal weight of the crystallographic term in the molecular dynamics refinement was used in the cycle. [b] All reflections $F > 2$ SD was used in the cycle.

determine the direction of the main chain or the orientation of the Glu^{124} and Asp^{127} side chains. The direction of the main chain in the model was finally built to maintain allowed backbone dihedral angles and to avoid close contacts with symmetry-related molecules. The lack of density may be a result of multiple conformations of the tip. The mean coordinate error was estimated by two methods. The coordinate error estimated from a σ_A plot (Read, 1986) in Figure 1 is 0.17 Å. The overall coordinate error as estimated by plotting the R factor as a function of resolution (Luzatti, 1952) lies between 0.17 and 0.20 Å when compared to theoretical curves for constant error (Fig. 2). The final refinement statistics for the current PelE and PelE-La^{3+} models are summarized in Table II.

The PelC model contains the first 352 residues of the mature protein, 128 water molecules and two sulfate ions. The model includes 103 of the 107 water molecules previously reported (Yoder and Jurnak, 1995). The PelC-Lu^{3+} model includes 352 amino acids, a Lu^{3+} ion, 132 water molecules, and 3 sulfate ions. The final refinement statistics for the current PelC and PelC-Lu^{3+} models are summarized in Table II.

Backbone Dihedral Angles

A Ramachandran plot (Ramachandran et al., 1963) of the backbone dihedral angles of the PelE model is shown in Figure 3. There is one *cis*-Pro in the structure, Pro^{232}. The density in this region is very clear, even in omit maps (Fig. 4A). *cis*-Pro^{232} is homologous to a *cis*-Pro in the analogous position in PelC. Of the 308 non-Gly and non-Pro amino acids, 261 (or 84.7%) lie in the most favored region of the plot and 14.3% lie in allowed regions. Two non-Gly residues, Phe^{236} and Asp^{173}, lie in the disallowed region. One non-Gly residue, Arg^{230}, lies in the generously allowed region. Phe^{236} lies in a short, tight turn between two β strands. Asp^{173} and Arg^{230} lie in a cleft formed at the junction of turn T3 and PB1. The electron density of the side chains of all three residues is very well resolved and

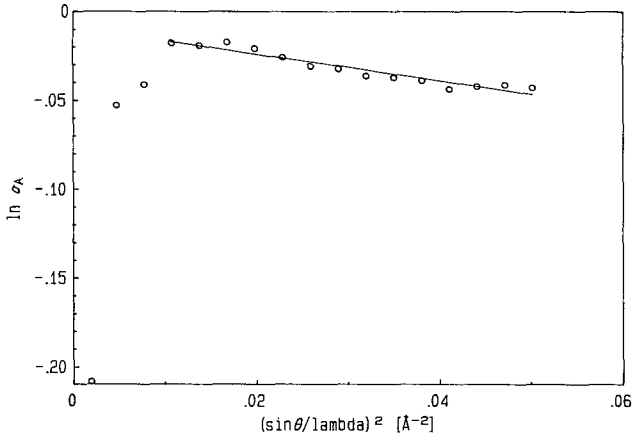

Figure 1. σ_A plot for the refined PelE model. The natural log of σ_A, the square of the correlation coefficient between the observed and calculated structure factor amplitudes, is plotted as a function of resolution shells. The mean coordinate error of the model, 0.02 Å, is calculated from the slope of the linear portion of the plot.

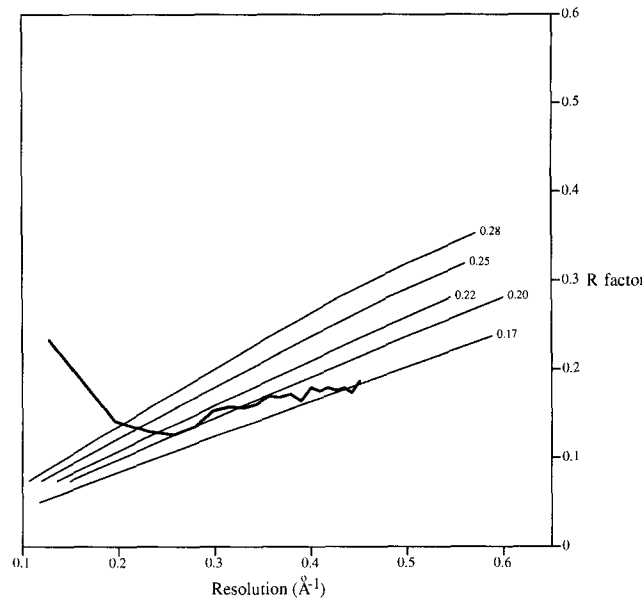

Figure 2. The crystallographic R factor plotted as a function of the resolution. The Luzatti plot for the final model of PelE is superimposed on theoretical curves assuming an average coordinate error of 0.17, 0.20, 0.22, 0.25, and 0.28 Å. The mean coordinate error of the PelE model lies between 0.20 and 0.22 Å and is a good agreement with the value for the σ_A plot.

the electron density for the Phe side chain is shown in Figure 4B.

Side-Chain Parameters

The side-chain density of all amino acids in the PelE model is clear except for seven surface residues: Lys^{26}, Lys^{62}, Thr^{65}, Asp^{68}, Thr^{284}, Asp^{285}, and Ser^{335}. The observed $\chi 1$ torsion angles in PelE agree well with the preferred conformers $g-(+60°)$, $t(+180°)$, and $g+(-60°)$ (Janin et al., 1978; Ponders and Richards, 1987). The average $\chi 1$ angles of the side chains of 289 residues, calculated by PROCHECK, are 58.7 ± 12.7, 183.4 ± 11.4, and −62.8 ± 9.8°, respectively, which correlate well with the values calculated by Morris et al. (1992) for well-defined structures at high resolution. The plot of $\chi 1$ versus $\chi 2$ in Figure 5 flags residues deviating more than 2.5 SD from the ideal position. Twenty-one of the 190 residues are flagged; many are Asps, which frequently have $\chi 1$ angles outside of the preferred conformers (Janin et al., 1978). The $\chi 3$ angle of the disulfide bridge is in a left-handed conformation with an angle of −83.1°. The analysis of the dihedral angles of side chains in the PelE structure indicates that the model is well refined.

Temperature Factors

Figure 6A displays the average B factor for the PelE model as a function of residue number. The average B factor is 15.3 $Å^2$ for all nonhydrogen protein atoms, 16.7 $Å^2$ for side-chain atoms, and 25.0 $Å^2$ for water molecules. Figure 6B illustrates the αC trace of PelE with the color of each residue specified by its average B factor. In general,

Table II. *Final water refinement statistics for PelE, the PelE-La^{3+} complex, PelC, and the PelC-Lu^{3+} complex*

Parameter	PelE	PelE-La^{3+}	PelC	PelC-Lu^{3+}
Resolution (Å)	2.2–10.0	2.2–10.0	2.2–10.0	2.2–10.0
Number of reflections ($F > 2$ SD)	17065	17147	25685	24971
Free R factor ($F > 2$ SD, 10% data)	22.0%	23.4%	22.3%	21.8%
Working R factor ($F > 2$ SD, 90% data)	15.7%	16.1%	17.2%	18.2%
Final R factor ($F > 2$ SD, 100% data)	16.1%	16.6%	17.5%	18.5%
Nonhydrogen protein atoms/asymmetric unit	2694	2694	2642	2642
Water molecules/asymmetric unit	157	163	128	132
SO_4^{2-} molecules/asymmetric unit	0	0	2	3
Cation/asymmetric unit	0	1	0	1
r.m.s. deviations from ideality in				
Bond length (Å)	0.009	0.009	0.008	0.007
Bond angle (°)	1.721	1.735	1.774	2.217
Improper angle (°)	1.180	1.205	1.199	1.353
Refined isotropic B factor for protein atoms				
Main chain atoms	13.99	14.65	19.41	20.12
All nonhydrogen protein atoms	15.29	15.25	20.46	20.91
All nonhydrogen atoms	15.82	16.51	21.40	22.47

the B factor correlates with the thermal motion of an atom and the higher ones are found in ambiguous or solvent-accessible regions. All regions with average B factors greater than 24.0 $Å^2$ are located in loops, including the ambiguous regions of PelE, Glu^{124} to Asp^{127} and Lys^{164} to Glu^{167}, and are indicated in red in Figure 6B. The regions that are best defined, with B factors less than 10.0 $Å^2$, mostly correspond to residues in the three β sheets and are shown in green in Figure 6B. It has been proposed that residues with the lowest B factors may represent the site of the protein-folding nucleus. Lumry and Gregory (1986), in a discussion of hydrogen exchange rates in proteins, predicted that the slow exchange core of the protein should be the residues with low crystallographic B factors. Subsequently, Kim et al. (1993) showed that the slow proton-exchanging core in bovine pancreatic trypsin inhibitor, typically three to eight residues, was the protein-folding core. Eleven residues with average B factors of less than 3.9 $Å^2$ include His^{148}, Val^{185}, Ile^{201}, Val^{217}, Thr^{218}, Asn^{222}, Ile^{239}, His^{240}, Ala^{241}, Phe^{261}, and Asn^{274} and are indicated in blue

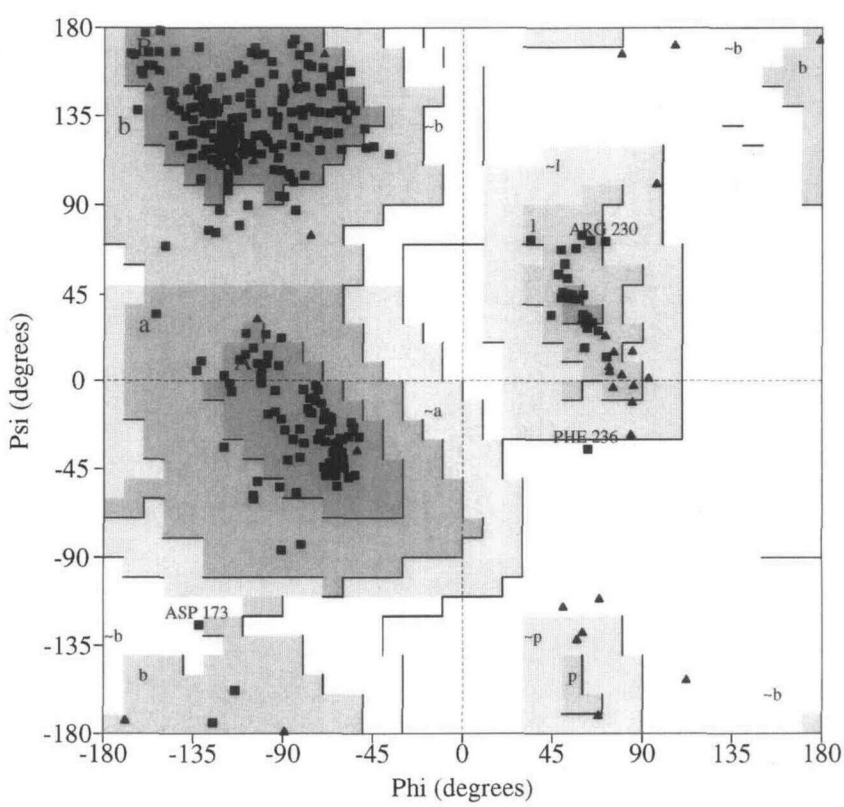

Figure 3. A plot of backbone dihedral angles, ϕ and ψ, for all nonterminal residues in the final model of PelE. Glys are indicated by triangles and all other residues are indicated by squares. Regions of the plot are represented by the shading with the darkest background indicating the region of the most favored ϕ and ψ values. The lightest region is disallowed. Amino acids in the generously allowed and disallowed regions are labeled.

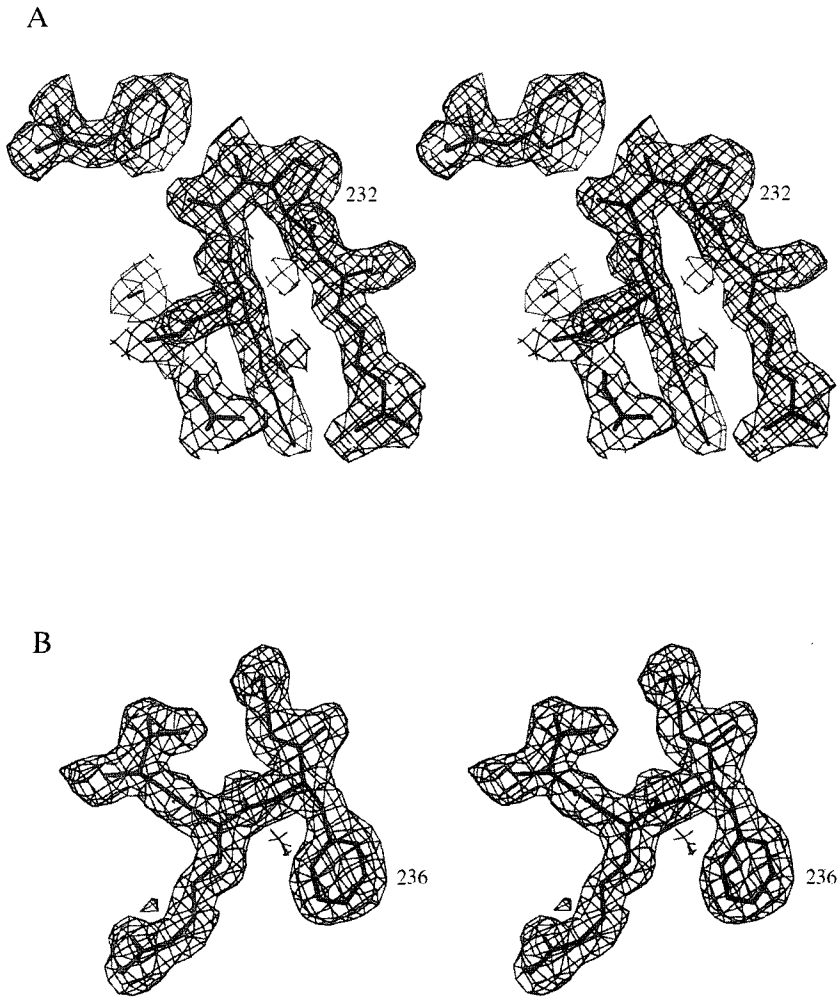

Figure 4. Stereo views of representative sections of the final $2F_o-F_c$ electron density map in which the model was omitted from a region around *cis*-Pro^{232} in A or around Phe^{236} in B. Both maps are contoured at 1.0 SD. The model is superimposed on the maps in black.

in Figure 6B. Nine of the 11 residues reside on five adjacent rungs of the parallel β helix, close to or within the repetitive T2 turn as defined in Figure 7.

Tertiary Structure of PelE

The PelE polypeptide backbone folds into a single structural domain, with dimensions of approximately 53 × 52 × 41 Å. The core of the protein is composed of three parallel β sheets whose individual parallel β strands coil up into a large right-handed cylinder, termed a parallel β helix. The N-terminal region of the protein forms a long loop, consisting of 26 amino acids that fold along one side of the parallel β helix and shield the interior of the protein from solvent. The protein then folds into the central parallel β helix domain. At the C-terminal end of the parallel β helix, the polypeptide folds into three distinct loops, one of which caps and shields the C-terminal end of the parallel β helix from solvent. The same loop, from Gly^{306} to Leu^{322}, is also bridged to an outer loop protruding from the parallel β helix by a disulfide bond between Cys^{291} and Cys^{320}. The C-terminal branch ends as a short α helix, Ser^{340} to Asn^{349}, followed by a hook, Ala^{350} to Leu^{355}. The core of the parallel β helix is formed by three parallel β sheets, PB1, PB2, and PB3, as shown in Figure 7. The three β sheets are composed of 6 to 10 β strands, and each β strand has two to five residues. The minimum number of amino acids in each turn of the parallel β helix is 22. The axial repeat per residue vertically along the central helix is 4.86 Å. The rise per residue is 0.22 Å and an αC-αC repeat distance of amino acids along the polypeptide chain within the core structure is 3.8 Å.

Secondary Structure

The amino acids that make up the secondary structural elements in the PelE model are listed in Table III. The molecule is predominantly β structure, with 93 amino acids (or 26.2%) classified as β strands, of which the vast majority (24.5%) is a parallel β secondary structure. PelE contains four α helices involving 8.4% of the amino acids and one short 3_{10} helix involving four (1.1%) amino acids. All of the helices are peripheral to the core of the structure.

Loops and β Turns

The loops, as defined by Ring et al. (1992), are summarized in Table IV. More than 60% of the residues in PelE are found

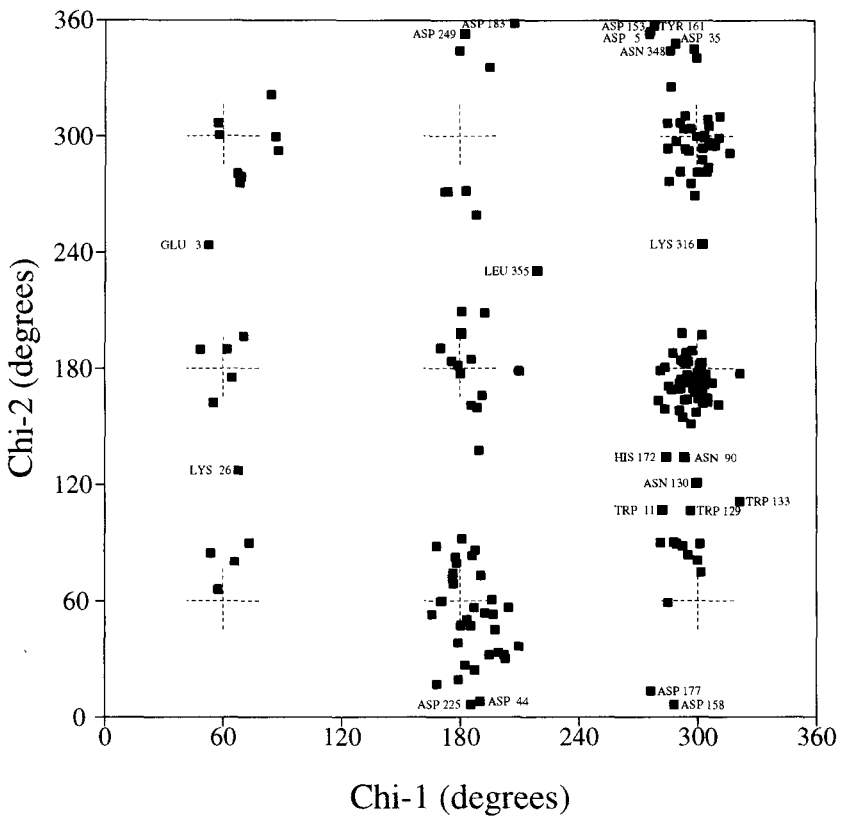

Figure 5. Plot of $\chi 1$ versus $\chi 2$ angles for 190 amino acids in PelE. The gauche$^-$, trans, and gauche$^+$ regions for $\chi 1$ and $\chi 2$ are represented by dashed crosses. The width of each cross is 1.0 SD. The points should cluster around the dashed crosses. Residues that deviate more than 2.5 SD from ideal are labeled.

in the N- and C-terminal branches or in the peptide connections of the parallel β helix. Together, PelE has six compound loops, consisting of both linear and nonlinear loops. One of the compound loops comprises the N-terminal branch from residues Ala^1 to Lys^{26}. The others are found at the T1 and T3 polypeptide connections within the parallel β helix, where T1 refers to the loops between β strands of PB1 and PB2, and T3, between PB3 and PB1, as shown in Figure 7. One of the 21 simple loops is found in the C-terminal branch, from residues Thr^{323} to Thr^{340}. The remaining 20 simple loops are found in the T1 or T3 connections and include 16 straps, one ω and three ζ loops. The strap regions of T1 and T3 are stabilized by many side-chain to main-chain and main-chain to main-chain hydrogen bonds. The T1 and the T3 regions vary considerably in size, from 4 to 23 residues, and in conformation for each rung of the parallel β helix in PelE. In contrast, the residues within each of 7 T2 polypeptide connections, between PB2 and PB3, maintain the same conformation throughout the parallel β helix. T2 forms a two-residue elbow turn with average ϕ and ψ angles of 56.7° and 34.3° for the first residue and −99.7 and 153.0° for the second residue. Because the average distance from αC_{i-1} to αC_{i+2} is 9.15 Å, longer than the comparable distance of 7.0 Å in four-residue $\gamma\beta_E$ turns characterized by Wilmot and Thornton (1990), the T2 turn in PelE is termed a distorted $\gamma\beta_E$ elbow turn.

Side-Chain-Stacking Interactions

The side-chain atoms of PelE show a high degree of organization, forming numerous linear stacking arrangements characterized by the types of amino acids found in the stack. Four different types of stacks are observed, including aromatic and ringed residue stacks, an Asn ladder, a Ser stack, and several aliphatic stacks. The longest stacks include the four-residue stack of Ile^{100}, Ile^{138}, Ile^{178}, and Ile^{210}; the four-residue stack of Phe^{192}, Phe^{224}, Tyr^{246}, and Phe^{276}; and the five-residue stack of Ser^{190}, Asn^{222}, Asn^{244}, Asn^{274}, and Ser^{307}. All side chains found within the interior of the parallel β helix and a few on the exterior surface are involved in side-chain-stacking interactions, which were discussed in more detail by Yoder et al. (1993b).

Charged Residues

PelE contains 26 Asp, 10 Glu, 8 Arg, and 29 Lys residues. The majority of the charged amino acids are solvent accessible and most are uniformly distributed over the surface of the protein. There is a small concentration of charges surrounding the Ca^{2+}-binding site. There are no charged residues in the interior of the parallel β helix, but two charged residues, Lys^{48} and Asp^{304}, occur in the N- and C-terminal coils of the parallel β helix and are solvent accessible. Three charged residues, Arg^{73}, Asp^{153}, and Asp^{211}, are buried in loops; these residues form a complete hydrogen bond network with other side-chain or main-chain atoms. The side-chain atoms of the charged residues form 10 salt bridges, which are listed in Table V. All are solvent exposed and all are formed by side chains extending outward from the parallel β helix. Asp^{183}, Lys^{214}, and Arg^{216} form a cluster of ionic interactions on an exposed surface of the parallel β

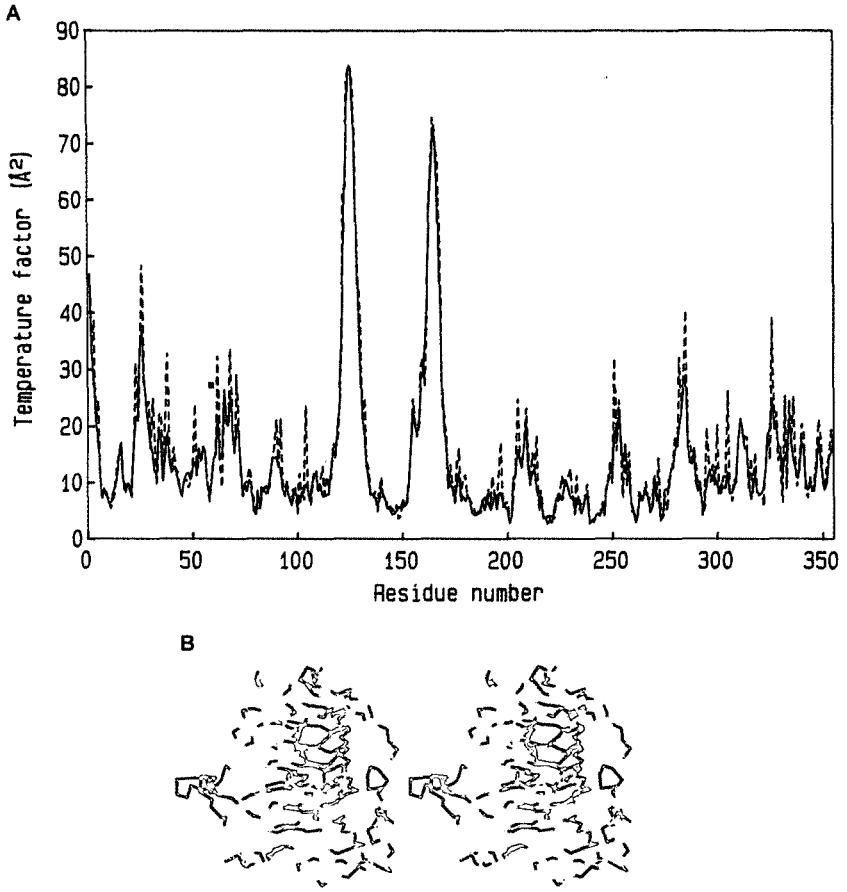

Figure 6. Representations of the refined temperature factors in the PelE model. A, The temperature factors are plotted as a function of residue number. The solid line indicates the average temperature factor of main-chain atoms and the dashed line is the average temperature factor of all nonhydrogen atoms. B, In the αC trace of PelE, the average temperature factor for each residue is coded by color. Residues with an average B factor greater than 24 Å^2 are in red, residues with B factors less than 10 Å^2 are illustrated in green, and the remaining residues with B factors between 10 and 24 Å^2 are in yellow. The residues with the 11 lowest B factors all lie within the parallel β-helix core and are illustrated in blue.

helix. Unlike PelC, the salt bridges are not found primarily in an extended groove around the Ca^{2+} site but are randomly distributed on the surface.

Protonation State of His

PelE has eight His's, three of which, His^{195}, His^{220}, and His^{240}, are clearly singly protonated. His^{195} forms hydrogen bonds with a main-chain carbonyl of Asp^{173} and the hydroxyl of Thr^{198}. The Nδ1 atom of His^{220} donates a hydrogen to Oδ1 of Asn^{22} and the Nε2 atom accepts a hydrogen from the hydroxyl group of Thr^{9}. In His^{240}, the hydrogen bonds are formed with the Oε1 atom of Glu^{272} and with the hydroxyl group of Tyr^{331}.

His^{148} is invariant in all Pels and, because it is part of the highly conserved vWiDH region, its hydrogen-bonding pattern has been carefully analyzed. The protonation state of His^{148} could either be single or double, depending on the rotation of the His ring. Both positions are compatible with the electron density. Crystal-packing interactions favor a double-protonation state because an extra hydrogen bond would be formed with a symmetry-related molecule. However, the crystal pH of 8 as well as a comparison with PelC favors a single-protonation state. If His^{148} is doubly protonated, then the Nδ1 atom of His^{148} forms a hydrogen bond with the carbonyl oxygen of Gly^{351} and the Nε2 atom, with the carbonyl oxygen of Ser^{206} in a symmetry-related molecule. In PelC, the analogous His is shielded from intermolecular contacts by a longer C-terminal loop. If the alternate position of the His ring in PelE is considered, then His^{148} is singly protonated in the PelE crystals. Nδ1 of His^{148} would then form a hydrogen bond with the Oδ2 atom of Asp^{147}, conserving a hydrogen bond interaction in the vWiDH region between two amino acids that are invariant in the Pel superfamily. In PelC crystals grown at a pH of 7, the analogous His is doubly protonated, donating its imidazole nitrogens to the invariant Asp in the vWiDH region and to a main-chain carbonyl oxygen in the longer C-terminal loop. The double-protonation state of His^{148} may be favored in PelE crystals but the single-protonation state is more likely to occur in solutions at a high pH. A comparison of the atomic details of the vWiDH region of PelE and PelC is shown in Figure 8.

Because the remaining His's are solvent accessible, the protonation states cannot be determined unambiguously. Nδ1 of His^{252} accepts a hydrogen from the main-chain nitrogen of Tyr^{225}, but Nε2 is oriented toward solvent. Nδ1 of His^{172} donates a hydrogen to Oδ2 of Asp^{158} and its Nε2 is oriented toward a water, Wat^{409}, but it is not clear whether the imidazole nitrogen is a hydrogen bond acceptor or donor. Similarly, Nε2 of His^{203} appears to form one hydrogen bond with the carbonyl oxygen of Leu^{355} in a

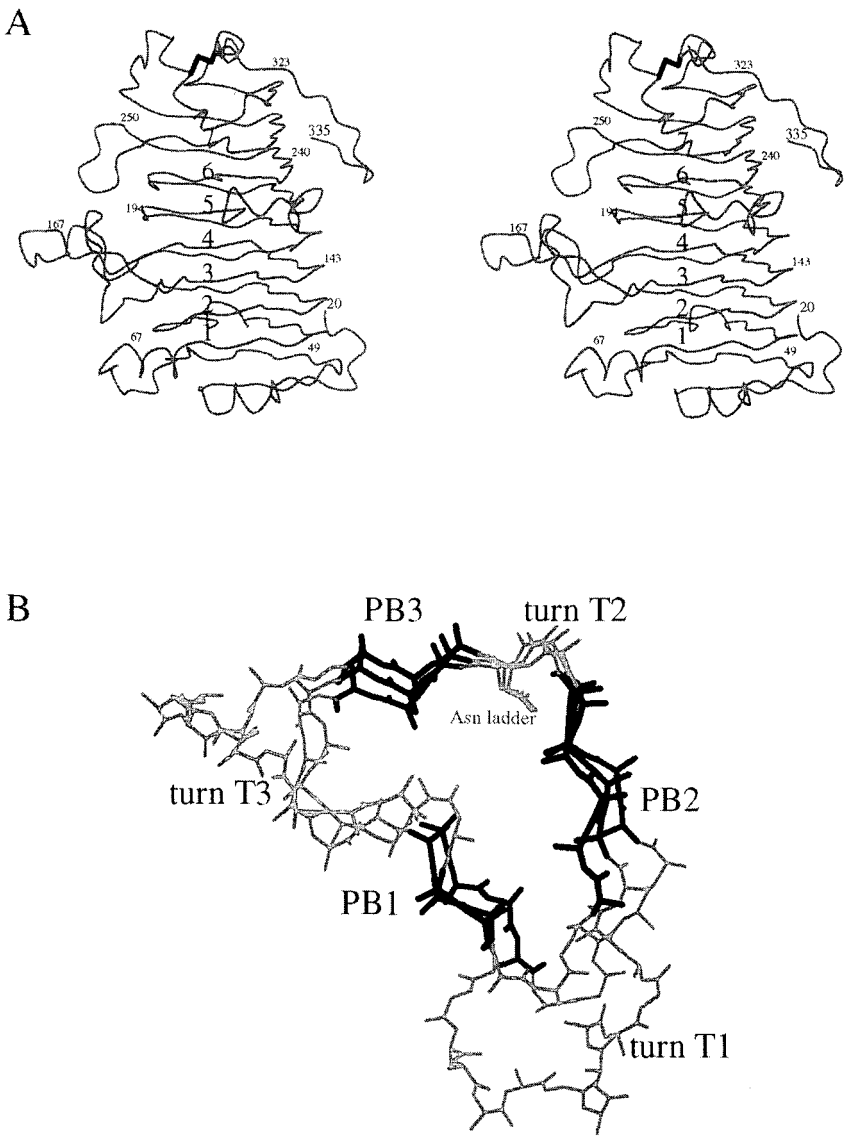

Figure 7. Illustration of the nomenclature used to describe the parallel β helix in PelE. A, The stereo view of an αC trace of PelE illustrates the seven coils of the parallel β-helix core with labels. The disulfide bond is illustrated by a thick black line. B, The cross-section of three coils of the parallel β helix is shown. The parallel β sheets, termed PB1, PB2, and PB3, are highlighted in black. The three turn regions, T1, T2, and T3, as well as the side chains of the Asn ladder, are shown in gray.

symmetry-related molecule and Nδ1 is oriented toward Wat^{429}. The side chain of His^{122} is completely solvent exposed and the protonation of its imidazole nitrogens cannot be determined.

Water Structure

The refined native PelE model contains 157 solvent molecules and all are assigned as waters. Of the 157 water molecules, 16 are buried water molecules with no solvent accessibility and have an average temperature factor of 11.4 Å^2. The buried water molecules are well ordered and are among the top peaks in the F_o-F_c electron density map used for assigning solvent molecules. Six of the buried water molecules are located within the core of the parallel β helix and the remaining 10 solvent-inaccessible water molecules are located on the exterior surface of the parallel β helix but are buried under protruding surface loops. All of the solvent-inaccessible water molecules are listed in Tables VI and VII. Four water molecules in the core, Wat^{489}, Wat^{490}, Wat^{491}, and Wat^{492}, form a network of water molecules in the region of PB3 and T3 between coils 6 and 7. One more water, Wat^{488}, forms a continuation of the network but is really outside of the parallel β-helix core. Wat^{488} is buried under a loop and is solvent inaccessible. Another water, Wat^{545}, is buried deep in the interior of the core. Wat^{545} bridges the hydroxyl of Tyr^{246}, part of an aromatic stack, and the carbonyl oxygen of Ala^{231}, which points toward the interior of the core but does not hydrogen bond with a main-chain atom from the T3 turn. The sixth water molecule in the core, Wat^{546}, forms three hydrogen bonds with main-chain atoms: the amide group of Gly^{96} and the carbonyl oxygens of Gly^{96} and Glu^{114}. Of the 16 buried water molecules, 14 form at least three hydrogen bonds, one with each hydrogen-bond acceptor and donor from the water molecule. The remaining two water molecules form only two apparent hydrogen bonds.

Table III. *Secondary structural elements in PelE*

Element	Designation[a]	Residues
Parallel β	PB2.1	27–30
	PB2.2	48–52
	PB1.1	76–78
	PB2.3	82–85
	PB1.2	97–100
	PB2.4	106–109
	PB3.1	112–113
	PB1.3	136–139
	PB2.5	144–147
	PB3.2	150–152
	PB1.4	176–179
	PB2.6	185–188
	PB3.3	191–193
	PB1.5	199–201
	PB2.7	217–220
	PB3.4	223–225
	PB1.6	233–234
	PB2.8	238–242
	PB3.5	245–247
	PB1.7	261–264
	PB2.9	268–272
	PB3.6	275–277
	PB1.8	294–296
	PB2.10	302–305
Antiparallel β		162–164
Helices	A	33–40
	B	67–74
	C	208–211
	D	289–292
	E	340–349

[a] Parallel β strands are named with a two-part label. The first part indicates the β sheet to which it belongs, if any. The second part is the sequential numbering of the β strand within that β sheet.

One hundred thirteen water molecules are part of the first hydration shell and form at least one hydrogen bond with a protein atom. The average B factor for the solvent-accessible water molecules is 26.2 $Å^2$, higher than that for the buried water molecules and consistent with greater thermal motion. Many of the external water molecules appear to stabilize loops and turns. For example, one external water molecule, Wat^{446}, forms a hydrogen bond with the carbonyl oxygen of Phe^{236} in a T1 turn at coil 6 of the parallel β helix. Phe^{236} is one of two non-Pro or non-Gly residues with a ϕ and a ψ angle in the disallowed region of the Ramachandran plot. There are no distinct patterns of hydration observed in the model and no regions in which the water molecules might form a network representing a possible substrate-binding site.

La^{3+} Inhibitor Studies

With an ionic radius of 1.016 Å, La^{3+} is often used as an analog of Ca^{2+}, which has a radius of 0.99 Å. La^{3+} and other lanthanide atoms have been used to study structural aspects of Ca^{2+} binding (Colman et al., 1972). As shown in Figure 9, the addition of $LaCl_3$ to an enzymatic assay in the presence of 0.5 mM $CaCl_2$ inhibits the activity of PelE. At a concentration of 0.05 mM $LaCl_3$, the enzymatic rate of PelE is reduced to 6% of the rate in the presence of 0.5 mM $CaCl_2$; at a concentration of 0.5 mM $LaCl_3$, the enzymatic reaction is abolished completely. That the inhibitory effect of La^{3+} on PelE activity is observed, despite a 10-fold excess of Ca^{2+}, suggests that La^{3+} has a stronger affinity for the protein. In data not shown, $LuCl_3$ has also been shown to inhibit the enzymatic activity of PelE at a concentration of 0.5 mM, but at a concentration of 0.05 mM, Lu^{3+} reduces the enzymatic rate of PelE to 69% of the rate in the presence of 0.5 mM $CaCl_2$. Thus, the inhibitory effect of Lu^{3+} is not as strong as that of La^{3+}.

Ca^{2+}/La^{3+}-Binding Site

Although Ca^{2+} is required for in vitro pectate lyase activity, its location on the enzyme or the substrate had not previously been established by biochemical methods. To determine whether a Ca^{2+}-binding site on PelE is possible, heavy atom derivatives, which frequently substitute at Ca^{2+} sites, have been used in the multiple isomorphous replacement phasing. Two of the derivatives, UO_2^{2-} and La^{3+}, share a common site that is located in a distinctive groove that lies parallel to the axis of the parallel β helix. To obtain a more accurate description of the site, a PelE-La^{3+} model was constructed and refined using the La^{3+} x-ray diffraction data set. The refined La^{3+} site is closely coordinated, with reasonable geometry and distance (Strynadka and James, 1989), with three carboxylic acid groups of two invariant aspartic acids: Oδ1 of Asp^{134} (2.72 Å), Oδ2 of Asp^{134} (2.90 Å), and Oδ1 of Asp^{177} (2.86 Å). A fourth ligand is provided by the carboxylic acid group of a conserved amino acid, Oδ1 of Asp^{173} (2.62 Å). Two additional ligands to the La^{3+} site are provided by water molecules, Wat^1 (2.34 Å) and Wat^4 (3.29 Å). Although the invariant residue, Arg^{230}, does not lie within the coordination sphere, the side chain is bridged to La^{3+} through a hydrogen-bonding network involving two water molecules, Wat^4 and Wat^5.

A superposition of the PelE and PelE-La^{3+} structures is shown in Figure 10A and the ligand distances are summarized in Table VIII. In the absence of any cation, as represented by the native PelE structure, there is minimal change in the orientation of any amino acids or water molecules directly coordinated with the cation-binding site in the PelE-La^{3+} complex. Given the arrangement of the six oxygen atoms, the La^{3+} site is believed to be a weak binding site for Ca^{2+} on the protein. This conclusion is also supported by the 1.8 Å resolution structure of *B.s.* Pel (Pickersgill et al., 1994) in which a Ca^{2+}-binding site is observed. In the latter structure, Ca^{2+} is coordinated with four protein ligands, analogous to those in PelE, and with three water molecules. One of the water molecules is analogous to Wat^1 found in the PelE structures. A close inspection of Figure 10A reveals that another change occurs in PelE upon the ligation of La^{3+}, but the change is only indirectly linked to the cation site. The side chain of the invariant Lys^{197} rotates toward the cation site in the PelE-La^{3+} structure and an additional water molecule, Wat^6, is present. The latter water molecule bridges Lys^{197} to Oδ2 of Asp^{173}, which is directly coordinated with the La^{3+} via Oδ1. Because of the minimal structural changes of PelE in

Table IV. *Loops and turns in PelE*

Loops are defined as all residues between secondary structural elements of the parallel β helix. If a four-residue β turn exists within a loop, the residue range and turn type, using the Wilmot-Thornton notation (1990), are listed.

Loop Range	Loop Type[a]	Region[b]	β Turn	
			Range	Type
1–26	Combination, 1–22 ζ 23–26 strap			
31–32	Strap			
41–48	ζ		41–44	εα
53–66	Combination, 53–62 ω 63–67 strap			
79–81	Strap	T1		
86–96	Combination, 86–91 ζ 92–96 strap		87–90	εα
101–105	Strap	T1		
110–111	Strap	T2	110–111	$\gamma\beta_E$
114–135	ζ	T3		
140–143	Strap	T1		
148–149	Strap	T2	148–149	$\gamma\beta_E$
153–175	Combination, 153–158 strap 159–175 ζ	T3	153–156 164–167	εα γγ
180–184	Strap	T1		
189–190	Strap	T2	189–190	$\gamma\beta_E$
194–198	Strap	T3		
202–216	Combination, 202–207 ω 212–216 ζ	T1		
221–222	Strap	T2	221–222	$\gamma\beta_E$
226–232	Strap	T3		
235–237	Strap	T1		
243–244	Strap	T2	243–244	$\gamma\beta_E$
248–260	ω	T3		
265–267	Strap	T1	265–267	$\beta_P\gamma$
273–274	Strap	T2	273–274	$\gamma\beta_E$
278–288	ζ		284–287	γγ
297–301	Strap	T1		
306–322	Combination, 312–318 strap 319–322 ω		309–312	γγ
323–340	ω			

[a] Loop type: strap (linear), ω (nonlinear, planar), ζ (nonlinear, nonplanar), or a combination of the three. [b] If applicable, region refers to the loops between the parallel β sheets as follows: T1 connects PB1 to PB2, T2 connects PB2 to PB3, and T3 connects PB3 to PB1.

the presence and absence of La^{3+}, it is difficult to explain the inhibitory effects of the lanthanide ions.

A binding site for Ca^{2+} is found at an analogous location in PelC by a similar analysis, superimposing the PelC and the PelC-Lu^{3+} complex structure as shown in Figure 10B. The refined Lu^{3+} site is closely coordinated with five carboxylic acid groups: Oδ1 of Asp^{129} (2.36 Å), Oδ1 of Asp^{131} (2.39 Å), Oδ2 of Asp^{131} (2.43 Å), Oε1 of Glu^{166} (2.38 Å), and Oδ2 of Asp^{170} (2.29 Å). Two additional ligands to the Lu^{3+} site are provided by water molecules, Wat^0 (1.92 Å) and Wat^3 (2.60 Å). The positions of Wat^0 and Wat^3 are analogous to two of the three coordinating water molecules in the *B.s.* Pel-Ca^{2+} structure. The most striking difference between PelC and the PelC-Lu^{3+} complex is the rotation of the Asp^{129} side chain from a noncoordinating position to one that strongly coordinates with Lu^{3+} at a distance of 2.36 Å. The side-chain movement apparently replaces a water molecule, Wat^1, found in metal-free PelC but not in the PelC-Lu^{3+} complex. Wat^1 is equivalent to one of the three coordinating water molecules in the *B.s.* Pel-Ca^{2+} structure. The second major difference is the identification of a sulfate ion in the PelC-Lu^{3+} structure at the position of Wat^2 in the PelC structure. Although the sulfate ion lies just outside the coordination sphere of the Lu^{3+}, it may contribute to charge neutralization of the cation in the PelC-Lu^{3+} structure and is not needed in the metal-free PelC structure. The third difference is a small rotation in the side chain of Glu^{166}, which forms a weak salt bridge with Lys^{190} (3.04 Å) in the PelC-Lu^{3+} complex but not in the metal-free PelC structure. As a consequence of the salt bridge, there is a shift in the side-chain conformations of Glu^{166} and Lys^{190}, resulting in a large movement of Oε1 of Glu^{166} away from the putative cation site in native PelC. Because of the structural differences of PelC in the presence and absence of Lu^{+3}, it appears that tighter binding of Lu^{+3} may account for its inhibitory effect.

A comparative analysis of the cation-binding sites in the PelE, PelC, and *B.s.* Pel metal complexes is complicated by the differences among the amino acids and water positions in the region. In general, each structure exhibits an exten-

Table V. *Salt bridges in PelE*

A salt bridge is defined as an interaction between charged groups of two amino acids. A hydrogen bond is when the donor-acceptor (D-A) distance is less than 3.9 Å, the hydrogen to acceptor (H-A) distance is less than 3.0 Å, and the angles defined by the donor to hydrogen to acceptor (D-H-A), the hydrogen to acceptor to acceptor-antecedent, and the donor to acceptor to acceptor-antecedent are all greater than 90.0°. Only the D-H-A angle is given.

Donor	Acceptor	D-A Distance	H-A Distance	D-H-A Angle
		Å	Å	°
Arg^{73} Nη2	Asp^{69} Oδ1	2.79	1.84	158.9
Arg^{73} Nε	Asp^{69} Oδ2	2.74	1.82	160.7
Lys^{101} Nξ	Asp^{139} Oδ1	3.07	2.33	126.7
Arg^{109} Nη1	Asp^{5} Oδ1	3.59	2.60	169.2
Arg^{109} Nε	Asp^{147} Oδ2	2.81	1.90	157.4
Lys^{214} Nξ	Asp^{183} Oδ1	2.98	2.05	148.1
Arg^{216} Nη2	Asp^{183} Oδ1	2.69	1.80	146.1
Arg^{216} Nε	Asp^{183} Oδ2	3.01	2.04	170.8
Arg^{226} Nη2	Asp^{225} Oδ1	3.06	2.11	158.7
Arg^{226} Nε	Asp^{225} Oδ2	3.15	2.25	151.4

sive network of water molecules, coordinating directly with the metal-binding site, as discussed, or forming an extensive hydrogen-bonding network with invariant and conserved amino acids in the metal-binding region. Many of the water positions are conserved, but none is invariant among all pectate lyase structures. A clear major difference among the three pectate lyase proteins is the presence of sulfate ions in the PelC structures, probably as a consequence of PelC crystallization conditions using 1.0 M or greater concentrations of ammonium sulfate. Two sulfate ions have been identified at comparable locations in both PelC and the PelC-Lu^{3+} complex. A third sulfate ion in the PelC-Lu^{3+} complex replaces a water molecule, Wat^{2}, in the metal-free PelC structure. As shown in Figure 11, the sulfate ions are separated by approximately 6.37 Å and form an arrangement compatible with the positions of three uronic acid moieties on each of three adjacent galacturonic acid units. Two oxygens of one sulfate, S1, lie within 3.9 Å of the Lu^{3+} site. One oxygen of the second sulfate, S2, is located 2.66 Å from N2 of the invariant Arg, Arg^{218}, and 3.34 Å from N1 of the same Arg. The third sulfate is close to Arg^{245} in PelC, with one oxygen located 2.25 Å from N1 and another located 3.17 Å from N2. Arg^{245} in PelC is spatially equivalent to Arg^{233} in PelE. The latter Args are invariant within the respective subfamily, *pelADE* or *pelBC*, but the sequence position is not invariant within the entire

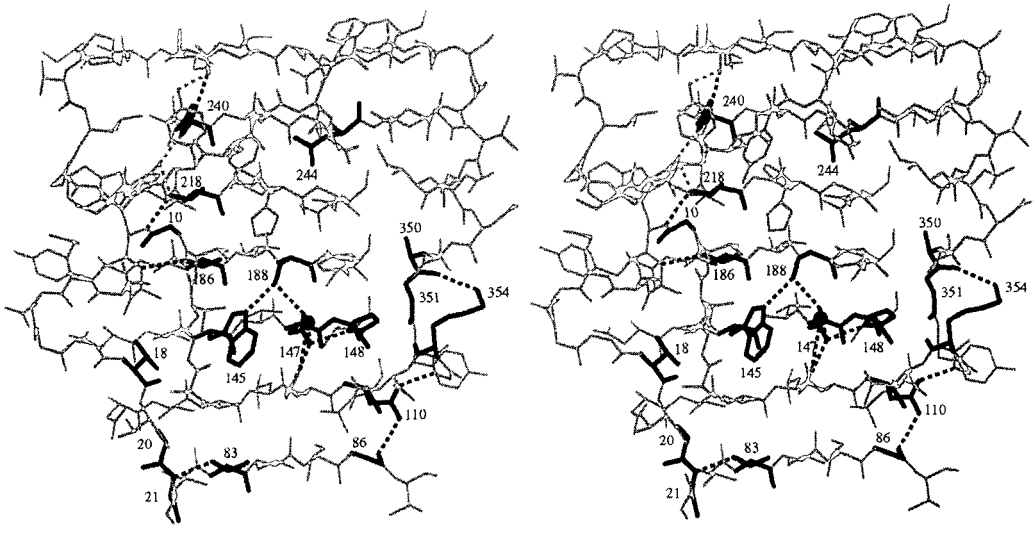

Figure 8. Stereo diagram of the atomic details of the vWiDH region of PelE assuming a single-protonation state of His^{148} as discussed in the text. The three-dimensional structure of the amino acids surrounding the vWiDH sequence is shown in gray. The amino acids that are invariant in the extracellular pectate lyase family are shown in black. The dashed lines indicate hydrogen bonds that are found in the refined structures of both PelE and PelC. The hydrogen bonds are illustrated in black if either the acceptor or donor is an invariant residue in the extracellular pectate lyase family or in gray if the acceptor or donor is an amino acid shared by PelE and PelC. The hydrogen bonds are formed between side-chain groups or between side-chain and main-chain atoms. Only one water molecule is conserved between PelE and PelC in the vWiDH region and is included in the diagram as a small black sphere.

Table VI. *Internal water molecules in PelE: water inside the core of the parallel β helix*

Water molecules (Wat) are numbered 401–557. The water oxygen atom is OH2, and the two hydrogen atoms are H1 and H2. For each internal water molecule, hydrogen bond donors for OH2 and hydrogen bond acceptors for H1 and H2 are listed.

Water No.	Hydrogen Bonds Formed from Water Atoms		
	OH2	H1	H2
489	Wat^{490} H1 Val^{227} NH	Wat^{488} OH2	Val^{227} O
490	Wat^{491} H1	Wat^{489} OH2	Leu^{247} O
491	Ser^{260} OH	Wat^{490} OH2	Wat^{492} OH2
492	Wat^{491} H2	Val^{227} O	Tyr^{259} O
545	Tyr^{246} OH	Ala^{231} O	
546	Gly^{96} NH	Gly^{96} O	Glu^{114} O

extracellular Pel family. Given the environment, the sulfates appear to mimic, although not perfectly, possible binding sites for three negatively charged uronic acid groups of the oligogalacturonic acid substrate.

The vWiDH Region

A number of investigators have noted that the vWiDH sequence pattern is shared by pectate lyases, pectin lyases, and plant homologs. More recently, a comparative sequence analysis of extracellular pectate lyases found that most of the invariant potentially catalytic amino acids cluster around the vWiDH region in PelE and PelC (Heffron et al., 1995; Henrissat et al., 1995). The observations suggest that the vWiDH region is probably an active site, although not necessarily the pectinolytic active site. The atomic details of PelE and PelC were compared to further elucidate the roles of the invariant amino acids in the vicinity of the vWiDH sequence. The side chains of all invariant amino acids are nearly identical with the positions highlighted in Figure 8 for PelE. In addition, the invariant residues participate in many hydrogen bonds, most of which are found in both PelE and PelC. The conserved intramolecular hydrogen bonds in the vWiDH region are listed in Table IX. It is interesting that the hydrogen bond between Oδ2 of Asp^{147} and the Nε of Arg^{109} in PelE is conserved even though the Arg is not. In all of the extracellular pectate lyases, only PelC is lacking an Arg in a comparable position. In PelC, the Arg is replaced by a Gln, Gln^{116}, which forms the conserved hydrogen bond with Oδ2 of Asp^{144}.

The positions of the refined water molecules in the PelE and the PelC structures were also compared. Not surprisingly, the refined water positions are virtually identical between the PelE and the PelE-La^{3+} structures and between PelC and the PelC-Lu^{3+} structures. However, there appears to be only one water position that is shared by both the PelE and PelC structures. This water molecule, as illustrated in Figure 8, forms a hydrogen bond with each carboxyl group of the invariant Asp, Asp^{147} in PelE or Asp^{144} in PelC. In the PelC structures, seven water molecules, including the one hydrogen bonded to Asp^{144}, form a continuous hydrogen bond network, giving the appearance of an oligopeptide β strand on the outer surface but parallel to the axis of the parallel β helix. An analogous water network is not observed in the PelE structures.

Table VII. *Internal water molecules in PelE: water molecules buried in loops or by side chains outside of parallel β-helix core*

Water molecules (Wat) are numbered 401–557. The water oxygen atom is OH2, and the two hydrogen atoms are H1 and H2. For each internal water molecule, hydrogen bond donors for OH2 and hydrogen bond acceptors for H1 and H2 are listed.

Water No.	Hydrogen Bonds Formed from Water Atoms		
	OH2	H1	H2
410	Asp^{173} H	Pro^{116} O	Trp^{133} O
411		Gln^{171} O	Trp^{133} O
414	Lys^{197} H	Wat^{415} OH2	Asp^{173} O
415	Wat^{414} H1	Asp^{153} Oδ1	Asp^{158} Oδ1
429	Lys^{180} H His^{203} Hδ1		Wat^{430} OH2
430	Ser^{204} H	Ser^{204} O	Asp^{211} Oδ2
480	Gly^{91} H	Gly^{88} O	Asn^{110} O
488	Wat^{489} H1 Asp^{249} NH	Asp^{249} O	Tyr^{255} O
530	Trp^{133} Hε2	Asp^{118} Oδ2	Gln^{70} Oε1
532	Thr^{162} H	Gln^{171} Oε1	Tyr^{169} O

DISCUSSION

The initial structural reports for PelE and PelC have revealed how the polypeptide backbone is folded into the unique parallel β helix, a topology not previously predicted or observed in the first 30 years of crystallography. Moreover, the localization of charged amino acids in a groove on PelE and PelC has provided the first indication of the locus of the pectinolytic active site. The present refined structures of PelE and PelC now provide accurate atomic coordinates, as demonstrated by standard crystal-

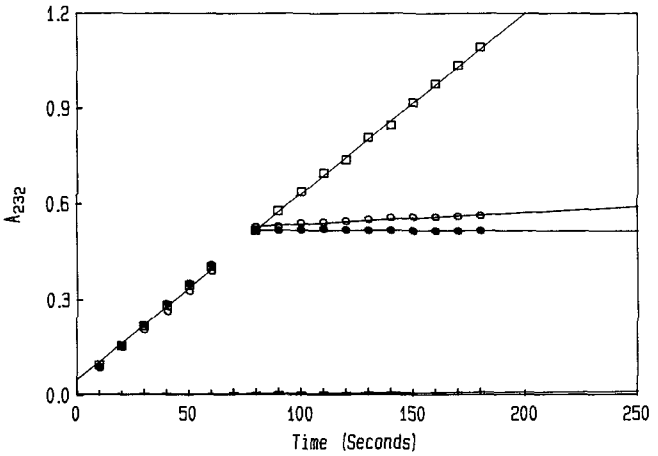

Figure 9. Enzymatic activity of PelE in the presence of $CaCl_2$ and/or $LaCl_3$. To a 0.995-mL solution containing 50 mM bis-Tris propane, pH 9.0, 1.25 mg/mL sodium polygalacturonate, and 0.5 mM $CaCl_2$, 2.4 pmol of PelE were added to initiate the reaction. A_{232} was recorded every 10 s. After 60 s, 0.005 mL of 0.1 M $CaCl_2$ (□), 0.005 mL of 0.1 M $LaCl_3$ (●), or 0.005 mL of 0.01 M $LaCl_3$ (○) was added to the assay. A standard activity assay substituting 0.5 mM $LaCl_3$ for the initial 0.5 mM $CaCl_2$ is shown in crosses.

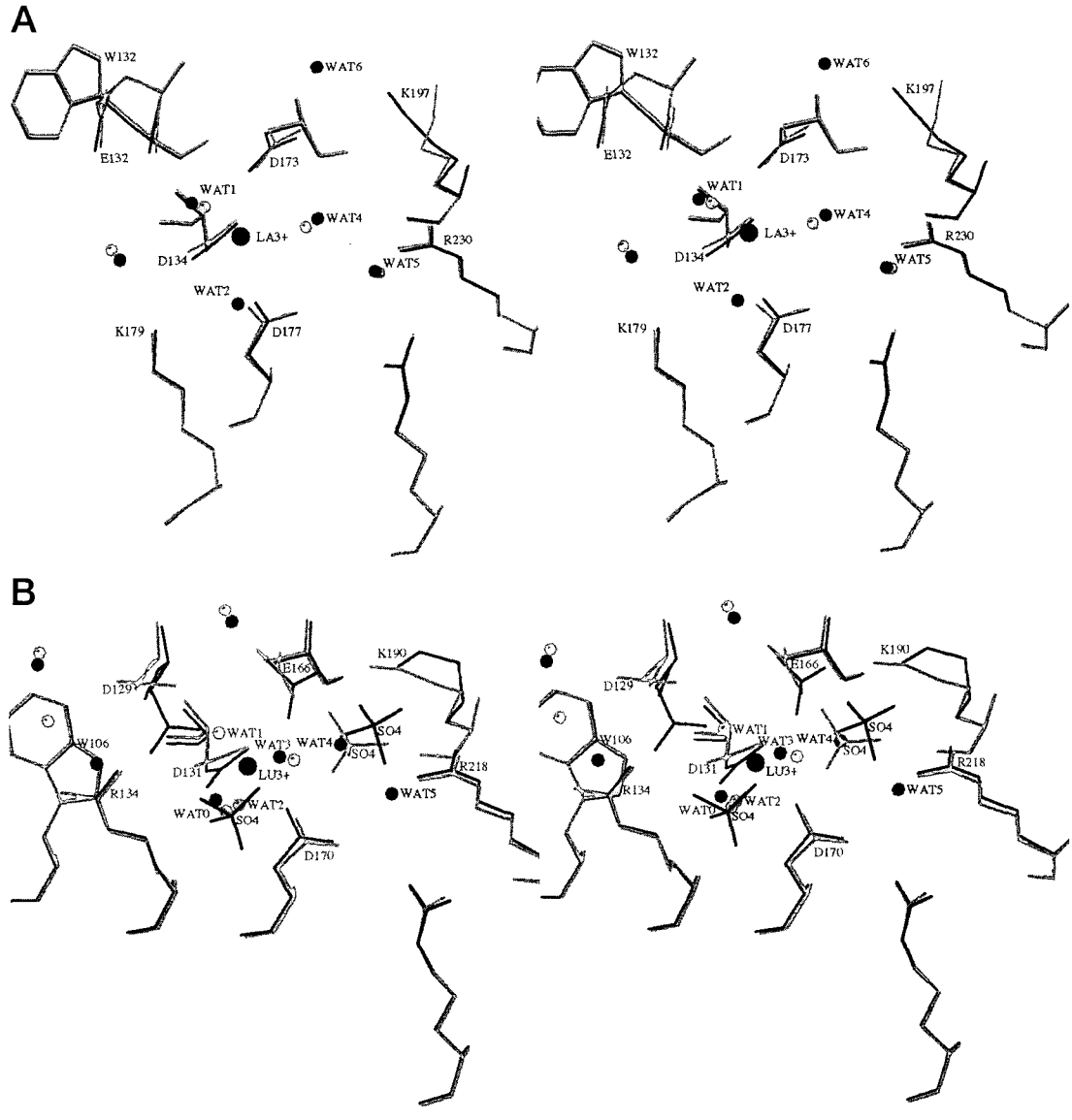

Figure 10. Stereo views of the superposition of the metal-free pectate lyase and the pectate lyase-M^{3+} complex in the region of the M^{3+}-binding site. The amino acids, water molecules, and sulfate ions surrounding the M^{3+} in the pectate lyase-M^{3+} complex are shown in black and the analogous region of the pectate lyase model is shown in gray. The water molecules are represented by small spheres and the M^{3+} is represented by a larger sphere. For comparative purposes the views are approximately the same as that for *B.s. Pel* in figures 7 and 8 of Pickersgill et al. (1994). A, Superposition of the PelE-La^{3+} complex and metal-free PelE. B, Superposition of the PelC-Lu^{3+} complex and metal-free PelC.

lographic criteria presented in Table II and in Figures 1 through 6. The atomic coordinates contain the details of all side-chain conformations as well as intramolecular interactions that stabilize each structure. A comparison of the atomic details of key regions of PelE and PelC has revealed the identification of shared features responsible for common functions. Concurrent with publication, the atomic coordinates for the four pectate lyase structures become accessible through the Brookhaven Protein Data Bank. Not only are the atomic coordinates useful for interpreting new biochemical data that become available for PelE and PelC, but they provide a foundation for modeling related pectate lyase structures or for designing genetic alterations to test hypotheses.

To obtain accurate atomic coordinates for each amino acid by current crystallographic techniques, it is necessary to include solvent molecules in the refinement. Without correct solvent placement, atoms within the amino acid side chains have a tendency to move into otherwise unassigned electron density. The placement of solvent positions becomes more reliable as the resolution of the x-ray diffraction data increases. At the 2.2 Å resolution of the current structural refinements, internal water molecules as well as water molecules within the first hydration shell

Table VIII. *Lanthanide coordinating ligands in PelE and PelC*

The distance from the La^{3+} ion to neighboring and coordinating ligands are given for the PelE-La^{3+} structure. The comparable distances are also given for the PelC-Lu^{3+} structure. In the uncomplexed PelE and PelC models, the comparable distances are provided, assuming the presence of a cation at the lanthanide ion atomic position.

PelE Ligand	PelE-La^{3+} Distance	PelE, Native Distance	PelC Ligand	PelC-Lu^{3+} Distance	PelC, Native Distance
	Å	Å		Å	Å
Glu^{132} Oε2	6.86	6.56	Asp^{129} Oδ1	2.36	5.12
Asp^{134} Oδ1	2.72	2.44	Asp^{131} Oδ1	2.39	2.10
Asp^{134} Oδ2	2.90	2.82	Asp^{131} Oδ2	2.43	2.56
Asp^{173} Oδ1	2.62	2.66	Glu^{166} Oε1	2.38	3.12
Asp^{177} Oδ1	2.86	2.56	Asp^{170} Oδ2	2.29	2.58
Wat^0 O			Wat^0 O	1.92	2.24
Wat^1 O	2.34	1.95	Wat^1 O		1.17
Wat^2 O	3.99		Wat^2 O		4.53
Wat^3 O			Wat^3 O	2.60	2.35
Wat^4 O	3.29	2.66	Wat^4 O	4.29	
			SO_4^1 S	4.45	

surrounding the protein can be placed with reasonable accuracy. These water molecules are placed not only by the presence of appropriately sized electron density but also by determining whether there are suitable hydrogen bond donors and acceptors near each water molecule. Because the diffraction resolution of neither PelE nor PelC extends to 2.0 Å or better, no attempt has been made to identify water molecules that might be present in hydrophobic pockets and thus are unable to form hydrogen bonds with neighboring groups.

In addition to improving the accuracy of the protein model, the inclusion of the solvent structure often reveals features of functional relevance. As expected, most water molecules in PelE and PelC lie within the first hydration shell at the protein-solvent boundary. A few water molecules are visible within the second hydration shell, forming hydrogen bonds to water molecules within the first hydration shell. Six water molecules in PelE and nine in PelC are also found within the core of the parallel β helix, forming hydrogen bonds to polar groups that otherwise could not pair with a suitable hydrogen-bonding partner. Similar internal, ordered water molecules are occasionally found in other proteins and usually contribute significantly to the stability of the structure. All water molecules, including internal ones, are continuously exchanging with those in the bulk solvent, albeit at different rates. Thus, it is somewhat surprising to find water molecules within the central core of PelE and PelC, because it implies that the parallel β helix is capable of opening and closing to permit the slow exchange of water molecules. Perhaps the most significant feature of any solvent structure is the identification of ordered solvent molecules in an active site region. Occasionally the solvent molecules form an outline of the substrate. Although no pattern reminiscent of an oligosaccharide could be detected in the pectinolytic active site region in any of the pectate lyase structures, continuous solvent density is observed in the vWiDH region of PelC and its complex with Lu^{3+}. The shape of the density is compatible with a polypeptide segment and is consistent with the hypothesis that the vWiDH region may participate in signal peptide cleavage (Jurnak et al., 1996).

The most significant finding of the refined structures is the elucidation of the atomic details of the metal-binding site, including the conformation of the coordinating amino acids, the ordered solvent structure in the region, and the extensive hydrogen-bonding network surrounding the site. The metal ion site is very important to the pectinolytic function of the enzymes, although its precise role remains an enigma. Ca^{2+} is essential for in vitro and probably in vivo catalytic cleavage of α-1,4-PGA by a β-elimination reaction (Collmer and Keen, 1986; Kotoujansky, 1987). The initial discovery of a metal-binding site on the pectate lyases has challenged the popular theory that Ca^{2+} binds only to the PGA substrate to keep it in an "eggbox" conformation that the enzyme could recognize (Gonzales-Candelas and Kolattukudy, 1992, and refs. therein). Clearly, the three pectate lyase structures demonstrate that this popular notion is incorrect. Now the major question has become, what precise role does Ca^{2+} play in catalysis? Does Ca^{2+} play a passive structural role in forming a saccharide-binding pocket as in concanavalin A (Hardman and Ainsworth, 1972) or does Ca^{2+} bind to the substrate directly as in C-type animal lectins (Weiss et al., 1992)? Does Ca^{2+} participate in catalysis directly, and if so, what function does the essential metal ion perform—neutralization of a negative charge, activation of a water molecule, or the lowering of a pK of a local group so that the proton abstraction and transfer steps of catalysis can be facilitated? The answer to the Ca^{2+} function is likely to require extensive and meticulous research.

Unfortunately, the present research does not address the central Ca^{2+} question directly because neither Ca^{2+} nor the substrate is present in the PelE or PelC crystals. However, Ca^{2+} has been replaced by a lanthanide ion in both structures, an observation that has led to the important discovery that the lanthanide compounds inhibit pectinolytic activity. Thus, two of the refined structures,

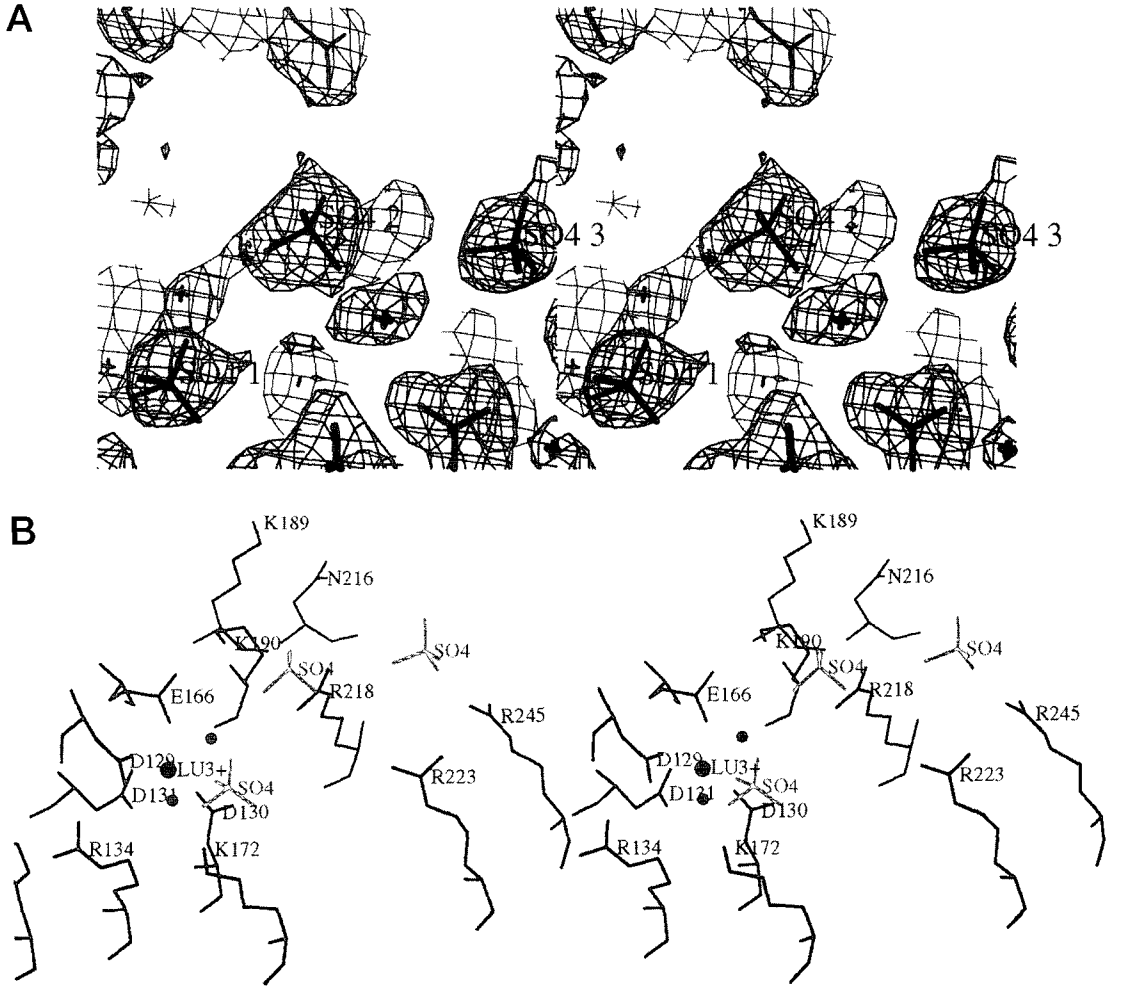

Figure 11. Stereo views of the sulfate positions in the PelC-Lu^{3+} complex. A, The final $2F_o$-F_c electron density map in which the model was omitted in a 10 Å shell around the Lu^{3+}. The map is contoured at 2 SD. B, The region around the Lu^{3+} in the PelC-Lu^{3+} model, illustrating the positions of the sulfate ions. In modeling studies the sulfate ions approximate the positions of three uronic acid moieties on adjacent galacturonate units.

PelE-La^{3+} and PelC-Lu^{3+}, represent the first views of pectate lyase-inhibitor complexes, providing clues to the structural features necessary for inhibition or activation. For the PelC-Lu^{3+} the answer is more obvious: the binding of Lu^{3+} causes a dramatic change in the orientation of several amino acids around the metal-binding site. Asp^{129} is oriented away in the apo form but rotates toward and coordinates directly with the Lu^{3+} in the complex. The second major change is the rotation of the side chain of Lys^{190}, which subsequently forms a weak ionic interaction with Glu^{166} in the PelC-Lu^{3+} complex, causing a stronger coordination of Glu^{166} through the carboxyl oxygen. With seven coordinating ligands, five from the protein and two from water molecules, Lu^{3+} appears to be more tightly bound than the Ca^{2+} found in the *B.s.* Pel-Ca^{2+} complex. Tighter coordination of a lanthanide ion may be responsible for inhibition if, indeed, some flexibility in Ca^{2+} coordination is required during catalysis. The reason for lanthanide inhibition is less clear for PelE, since only small changes are observed in the coordination sphere of the metal ion: the side chain of Lys^{197} rotates toward Asp^{173} and forms a hydrogen bond through an extra water molecule. Thus, the only structural change in common is the rotation of Lys^{197} in PelE or the analogous Lys^{190} in PelC upon complexation with a lanthanide ion. These observations underscore the significance of the proper orientation for this particular Lys, an invariant amino acid in the pectate lyase subfamily but not in the pectin lyases or plant pollen homologs.

A comparison of the solvent structures in PelE-La^{3+}, PelC-Lu^{3+}, and *B.s.* Pel-Ca^{2+} reveals that most water positions are highly conserved but not invariant as a consequence of subtle changes in the amino acids surrounding the metal ion site. Only two water molecules, Wat^4 and Wat^5, are invariant, both of which form hydrogen bonds with the invariant Arg. In PelC-Lu^{3+}, Wat^4 bridges the invariant Arg to the Ca^{2+} through another water molecule,

Table IX. *Conserved intramolecular interactions in the vWiDH region of PelE*

For the comparison the single-protonation state of His^{148} is assumed. The amino acids that are invariant in all extracellular pectate lyases are highlighted in boldface.

PelE			PelC
Donor	Acceptor	Donor-acceptor distance	Analogous residues
		Å	
Thr^{83} OG1	**Gly^{21}** N	2.85	**Thr^{92}–Gly^{13}**
Arg^{109} Nε	**Asp^{147}** Oδ1	2.81	Gln^{116}–**Asp^{144}**
Asn^{110} Nδ2	**Gly^{86}** O	2.98	**Asn^{117}–Gly^{95}**
Asn^{110} Oδ2	Gly^{353} N	2.67	**Asn^{117}**–Gly^{341}
Trp^{145} Nε1	**Ser^{188}** OG	2.88	**Trp^{144}–Ser^{181}**
His^{148} Nε1	**Asp^{147}** Oδ1	2.82	**His^{145}–Asp^{144}**
Thr^{186} OG1	Ala^{12} N	3.08	**Thr^{179}**–Ala^{8}
Ser^{188} OG	**Asp^{147}** Oδ2	2.96	**Ser^{181}–Asp^{144}**
Thr^{218} OG1	Trp^{11} N	3.01	**Thr^{206}**–Tyr^{7}
Tyr^{331} OH	**Thr^{218}** OG1	2.91	Tyr^{320}–**Thr^{206}**
Tyr^{331} OH	**His^{240}** Nδ1	2.62	Tyr^{320}–**His^{228}**
Glu^{272} Oε2	**His^{240}** Nε2	3.08	Glu^{232}–**His^{228}**
Tyr^{333} OH	Glu^{272} Oε2	2.64	Tyr^{322}–Glu^{272}
Lys^{354} Nξ	**Ala^{350}** O	3.42	**Lys^{342}–Ala^{338}**

Wat^{3}. These water molecules may represent substrate structure or may play a critical role in catalysis. Another striking feature of the ordered water structure around the metal ion site is the extensive hydrogen bond network, linking the water molecules with the invariant and conserved amino acids in the region.

An unexpected caveat in the high-resolution refinement is the tentative identification of sulfate molecules in the PelC and PelC-Lu^{3+} structures, probably a result of the high concentration of ammonium sulfate in the crystallization media. The identification from electron density size and environment is possible only as a consequence of the correct positioning of other water molecules in the region. The sulfates are located near the Ca^{2+} site, surrounded by invariant or conserved positively charged amino acids. They form an arrangement compatible with the positions of the uronic acid moiety in a conformation of PGA elucidated by fiber diffraction studies (Walkinshaw and Arnott, 1981). In the PelC-Lu^{3+} complex an extra sulfate is located very close to the metal ion. If the metal ion were Ca^{2+} or the sulfate geometry closer to trigonal, it is not difficult to imagine that the anion might represent a uronic acid moiety coordinating directly with the Ca^{2+}. Thus, Ca^{2+} may be shared by the enzyme and the substrate, serving to neutralize the negative charge on an uronic acid group of the substrate. Because there is only one common Ca^{2+} site detected in each pectate lyase structure, but several negatively charged groups on the substrate, Ca^{2+} may also serve to properly position an important uronic acid group, possibly the one that neighbors the glycosidic scissile bond. Although there are yet many feasible arrangements of an oligogalacturonate substrate in the putative binding site, the sulfate positions should limit the possibilities in future modeling experiments.

Sequence alignments of the extracellular pectate lyase superfamily have suggested that two amino acids in the Ca^{2+}-binding region play a key role in oligosaccharide cleavage. The amino acids are Asp^{134} and Arg^{230} in PelE and Asp^{131} and Arg^{218} in PelC. In all three Pel structures the invariant Asp binds strongly to the Ca^{2+}, coordinating through both carbonyl oxygens. The Arg is linked to the cation site through two water molecules. Despite the structural information, the functional roles of the two amino acids are not clear. In other saccharidases, aspartic or Glu groups usually initiate proton abstraction. Because the invariant Asp is tightly coordinated through both carbonyl groups with the Ca^{2+} in the pectate lyases, it is difficult to understand how this amino acid could also be responsible for proton abstraction. One possibility is that one of the two carbonyl groups is simultaneously released from Ca^{2+} coordination as the negatively charge uronic acid moiety of PGA binds to the Ca^{2+}.

In the PelC-Lu^{3+} structure the invariant Arg Arg^{218} interacts with a sulfate group and suggests that its role, like Ca^{2+}, may be neutralization of a negatively charged uronic acid moiety. However, the latter explanation does not provide a plausible common enzymatic mechanism for pectin lyases, another enzyme class belonging to the extracellular Pel superfamily. Pectin lyases cleave the neutral, methylated form of PGA and do not require Ca^{2+} for activity. If all lyases, including the pectate and pectin lyases, share a similar enzymatic mechanism as postulated (Gacesa, 1987), then the invariant Arg must serve a role that is shared by all enzyme families. Such a role may involve protonation of the carbonyl oxygen as the proton is abstracted from C_5 during the β-elimination cleavage of PGA (Gerlt and Gassman, 1992). Eventually, a proton must be donated to the glycosidic oxygen of the cleaved bond. Rather than invoke a single proton donor, the extensive network of hydrogen bonds around the Ca^{2+} site suggests a mechanism whereby a proton is transferred from C_5 of PGA via several residues and/or water molecules to the glycosidic oxygen.

Received September 5, 1995; accepted January 12, 1996.

LITERATURE CITED

Baker EN, Hubbard RE (1984) Hydrogen bonding in globular proteins. Prog Biophys Mol Biol **44:** 97–179

Barras F, Thurn KK, Chatterjee AK (1987) Resolution of four pectate lyase structural genes of *Erwinia chrysanthemi* (EC16) and characterization of the enzymes produced in *Escherichia coli*. Mol Gen Genet **209:** 319–325

Barras F, van Gijsegem F, Chatterjee AK (1994) Extracellular enzymes and pathogenesis of soft-rot *Erwinia*. Annu Rev Phytopathol **32:** 201–234

Bernstein FC, Koetzle TF, Williams GJB, Meyer EF, Brice MD, Rodgers JR, Kennard O, Shimanouchi T, Tasumi M (1977) The protein data bank: a computer-based archival file for macromolecular structures. J Mol Biol **112:** 535–542

Bhat TN, Cohen GH (1984) OMITMAP: an electron density map suitable for the examination of errors in a macromolecular model. J Appl Crys **17:** 244–248

Brünger AT (1988) Crystallographic refinement by simulated annealing: application to a 2.8 Å resolution structure of aspartate aminotransferase. J Mol Biol **208:** 803–816

Brünger AT (1991) Simulated annealing in crystallography. Annu Rev Phys Chem **42:** 197–223

Brünger AT (1992) X-PLOR, version 3.0. Yale University, New Haven, CT

Brünger AT (1993) Assessment of phase accuracy by cross validation: The free R value. Methods and applications. Acta Crystallogr Sect D **49:** 24–36

Budelier KA, Smith AG, Gasser CS (1990) Regulation of a stylar transmitting tissue-specific gene in wild-type and transgenic tomato and tobacco. Mol Gen Genet **224:** 183–192

Collmer A, Keen NT (1986) The role of pectic enzyme in plant pathogenesis. Annu Rev Phytopathol **24:** 383–409

Colman PM, Weaver LH, Matthews BW (1972) Rare earths as isomorphous calcium replacements for protein crystallography. Biochem Biophys Res Commun **46:** 1999–2004

Engh R, Huber R (1991) Accurate bond and angle parameters for x-ray protein structure refinement. Acta Crystallogr Sect A **47:** 392–400

Fitzgerald P, Madsen N (1986) Improvement of limit diffraction and useful x-ray lifetime of crystals of glycogen debranching enzyme. J Crystal Growth **76:** 600–606

Gacesa P (1987) Alginate-modifying enzymes. A proposed unified mechanism of action for the lyases and epimerases. FEBS Lett **212:** 199–202

Gerlt J, Gassman P (1992) Understanding enzyme-catalyzed proton abstraction from carbon acids: details of stepwise mechanism for β-elimination reactions. J Am Chem Soc **114:** 5928–5934

Gonzales-Candelas L, Kolattukudy PE (1992) Isolation and analysis of a novel inducible pectate lyase gene from the phytopathogenic fungus *Fusarium solani* f. sp. *pisi* (*Nectria haematococca*, mating population VI). J Bacteriol **174:** 6343–6349

Gysler C, Harmesen JA, Kester HC, Vissar J, Heim J (1990) Isolation and structure of the pectin lyase D-encoding gene from *Aspergillus niger*. Gene **89:** 101–108

Hardman KD, Ainsworth CF (1972) Structure of concanavalin A at 2.4Å resolution. Biochemistry **11:** 4910–4919

Heffron S, Henrissat B, Yoder MD, Lietzke SE, Jurnak F (1995) Structure-based multiple alignment of extracellular pectate lyase sequences. Mol Plant-Microbe Interact **8:** 331–334

Henrissat B, Heffron SE, Yoder MD, Lietzke SE, Jurnak F (1995) Functional implications of structure-based sequence alignment of proteins in the extracellular pectate lyase superfamily. Plant Physiol **107:** 963–976

Hinton JCD, Sidebotham JM, Gill DR, Salmond GPD (1989) Extracellular and periplasmic isoenzymes of pectate lyase from *Erwinia carotovora* subspecies *carotovora* belong to different gene families. Mol Microbiol **3:** 1785–1795

Hodel A, Kim SH, Brünger AT (1992) Model bias in macromolecular crystal structures. Acta Crystallogr Sect A **48:** 851–858

Hugouvieux-Cotte-Pattat N, Robert-Baudouy J (1992) Analysis of the regulation of the pelBC genes in *Erwinia chrysanthemi* 3937. Mol Microbiol **6:** 2363–2376

Janin J, Wodak S, Levitt M, Maigret B (1978) Conformation of amino acid side-chains in proteins. J Mol Biol **125:** 357–386

Jones TA (1985) Interactive computer graphics: FRODO. Methods Enzymol **115:** 157–171

Jones TA, Zou JY, Cowan SW, Kjeldgaard M (1991) Improved methods for building protein models in electron density maps and the location of errors in these models. Acta Crystallogr Sect A **47:** 110–119

Jurnak F, Kita N, Garrett M, Heffron SE, Scavetta R, Boyd C, Keen N (1996) Functional implications of the three-dimensional structures of pectate lyases. *In* J Visser, ed, Pectins and Pectinases, Symposium Proceedings. Elsevier Science, New York (in press)

Kabsch W, Sander C (1983) Dictionary of protein secondary structure: pattern recognition of hydrogen bonded and geometrical features. Biopolymers **22:** 2577–2637

Keen NT, Dahlbeck D, Staskawicz B, Belser W (1984) Molecular cloning of pectate lyase genes from *Erwinia chrysanthemi* and their expression in *Escherichia coli*. J Bacteriol **159:** 825–831

Kim C-Y, Mosser V, Keen NT, Jurnak F (1989) Preliminary crystallographic analysis of a plant pathogenic factor: pectate lyase E. J Mol Biol **208:** 365–367

Kim K-S, Fuchs JA, Woodward CK (1993) Hydrogen exchange identifies native-state motional domains important in protein folding. Biochemistry **32:** 9600–9608

Kotoujansky A (1987) Molecular genetics of pathogenesis by soft-rot *Erwinias*. Annu Rev Phytopathol **25:** 405–430

Kuster-van Someren M, Flipphi M, de Graff L, van den Broeck H, Kester H, Hinnen A, Visser J (1992) Characterization of the *Aspergillus niger pel*B gene: structure and regulation of expression. Mol Gen Genet **234:** 113–120

Laskowski RA, MacArthur MW, Moss DS, Thorton JM (1992) PROCHECK: a program to check the stereochemical quality of protein structures. J Appl Crystallogr **26:** 283–291

Lesczynki JF, Rose GD (1986) Loops in globular proteins: a novel category of secondary structure. Science **234:** 849–855

Lietzke SE, Yoder MD, Keen NT, Jurnak F (1994) The three-dimensional structure of pectate lyase E, a plant virulence factor from *Erwinia chrysanthemi*. Plant Physiol **106:** 849–862

Lumry R, Gregory RB (1986) Free-energy management in protein reactions: concepts, complications, and compensation. *In* GR Welch, ed, The Fluctuating Enzyme. Wiley Interscience, New York, pp 1–190

Luzatti V (1952) Traitement statistique des errerus dans la determination des structures cristallines. Acta Crystallogr **5:** 802–810

McDonald IK, Naylor DN, Jones DT, Thornton JM (1993) HBPLUS. Department of Biochemistry and Molecular Biology, University College, London

Morris AL, MacArthur MW, Hutchinson EG, Thornton JM (1992) Stereochemical quality of protein structure coordinates. Proteins **12:** 345–364

Pickersgill R, Jenkins J, Harris G, Nasser W, Robert-Baudouy J (1994) The structure of *Bacillus subtilis* pectate lyase in complex with calcium. Nat Struct Biol **1:** 717–723

Ponders JW, Richards FM (1987) Tertiary templates for proteins. Use of packing criteria in the enumeration of allowed sequences for different structural classes. J Mol Biol **193:** 775–791

Powell NJD (1977) Restart procedures for the conjugate gradient method. Mathematical Programming **12:** 241–254

Preston JF III, Rice JD, Ingram LO, Keen NT (1992) Differential depolymerization mechanisms of pectate lyases secreted by *Erwinia chrysanthemi* EC16. J Bacteriol **174:** 2039–2042

Rafner T, Griffith IJ, Kuo MC, Bond JF, Rogers BL, Klapper DG (1991) Cloning of *Amb a I* (antigen E), the major family of short ragweed pollen. J Biol Chem **266:** 1229–1236

Ramachandran GN, Ramakrishnan C, Sasisekharan V (1963) Stereochemistry of polypeptide chain configuration. J Mol Biol **7:** 95–99

Read RJ (1986) Improved Fourier coefficients for maps using phases from partial structures with errors. Acta Crystallogr Sect A **42:** 140–149

Ring CS, Kneller DG, Langridge R, Cohen FE (1992) Taxonomy and conformational analysis of loops in proteins. J Mol Biol **224:** 685–699

Rogers HJ, Harvey A, Lonsdale DM (1992) Isolation and characterization of a tobacco gene with homology to pectate lyase which is specifically expressed during microsporogenesis. Plant Mol Biol **20:** 493–502

Strynadka NCJ, James MNG (1989) Crystal structures of the helix-loop-helix calcium binding proteins. Annu Rev Biochem **58:** 951–958

Tamaki SJ, Gold S, Robeson M, Manulis S, Keen NT (1988) Structure and organization of the *pel* genes from *Erwinia chrysanthemi* EC16. J Bacteriol **170:** 3468–3478

Walkinshaw MD, Arnott S (1981) Conformations and interactions of pectins. I. X-ray diffraction analyses of sodium pectate in neutral and acidified forms. J Mol Biol **153:** 1055–1073

Weiss WI, Drickamer K, Hendrickson WA (1992) Structure of a C-type mannose-binding protein complexed with an oligosaccharide. Nature **360:** 127–134

Wilmot CM, Thornton JM (1990) β-Turns and their distortions: A proposed new nomenclature. Protein Engin **3:** 479–493

Wing RA, Yamaguchi J, Larabell SK, Ursin VM, McCormick S (1989) Molecular and genetic characterization of two pollen-expressed genes that have sequence similarity to pectate lyases of the plant pathogen *Erwinia*. Plant Mol Biol **14:** 17–28

Yoder MD, Jurnak F (1995) The refined three-dimensional structure of pectate lyase C from *Erwinia chrysanthemi* at 2.2 Å resolution. Implications for an enzymatic mechanism. Plant Physiol **107:** 349–364

Yoder MD, Keen NT, Jurnak F (1993a) New domain motif: the structure of pectate lyase C, a secreted plant virulence factor. Science **260:** 1503–1507

Yoder MD, Lietzke SE, Jurnak F (1993b) Unusual structural features of the parallel β helix of the pectate lyases. Structure **1:** 241–251

Zucker M, Hankin L (1970) Regulation of pectate lyase synthesis in *Pseudomonas fluorescens* and *Erwinia carotovora*. J Bacteriol **104:** 13–18